Alternative splicing in mechanically stretched podocytes as a model of glomerular hypertension

Francescapaola Mattias[1], Olga Tsoy[2], Elke Hammer[3], Alexander Gress[4], Stefan Simm[5,6], Chit Tong Lio[7], Sabine Ameling[3], Olga Kalinina[4], Kerstin Amann[8], Leonie Dreher[9], Ulrich Wenzel[9], Karlhans Endlich[1], Jan Baumbach[2], Uwe Völker[3], Nicole Endlich[1,10#], Felix Kliewe[1*#]

[1] Department of Anatomy and Cell Biology, University Medicine Greifswald, Greifswald, Germany
[2] Institute for Computational Systems Biology, University of Hamburg, Hamburg, Germany
[3] Interfaculty Institute for Genetics and Functional Genomics, University Medicine Greifswald, Greifswald, Germany
[4] Department of Drug Bioinformatics, Helmholtz Institute for Pharmaceutical Research Saarland (HIPS), Helmholtz Centre for Infection Research (HZI), Saarbrücken, Germany
[5] Institute of Bioinformatics, University Medicine Greifswald, Greifswald, Germany
[6] Coburg University of Applied Sciences, Institute of Bioanalysis, Coburg, Germany
[7] Data Science in Systems Biology, Technical University of Munich, Freising, Germany
[8] Department of Nephropathology; Friedrich-Alexander University (FAU) Erlangen-Nuremberg, Erlangen, Germany
[9] III. Department of Medicine, University Hospital Hamburg-Eppendorf, Hamburg, Germany
[10] NIPOKA GmbH, Center of High-End Imaging, Greifswald, Germany

# These authors contributed equally

[*] Corresponding author:

Dr. Felix Kliewe

Institut für Anatomie und Zellbiologie, Universitätsmedizin Greifswald

Friedrich-Loeffler-Str. 23c, 17489 Greifswald, Germany

Email: felix.kliewe@uni-greifswald.de, Phone: +49 (0)3834 86-5315

Abstract

Alterations in pre-mRNA splicing play an important role in disease pathophysiology. However, the role of alternative splicing (AS) for podocytes in hypertensive nephropathy (HN) has not been investigated. The purpose of the Sys_CARE project was to identify AS events that play a role in the development and progression of HN. For this, murine podocytes were exposed to mechanical stretch, after which proteins and mRNA were analyzed by proteomics, RNA-Seq and several bioinformatic AS tools.

Based on transcriptomics and proteomics analysis we could observe significant changes in gene expression and abundance of proteins under mechanical stretch compared to unstretched conditions. By RNA-Seq, we identified over 1000 different splicing events including all types of AS events. We identified 17 genes that showed an AS event in four different splicing analysis tools. We focused on *Myl6*, a component of the myosin protein complex, and *Shroom3*, an actin-binding protein crucial for podocyte function. We found two *Shroom3* isoforms that showed significant changes in expression upon mechanical stretch, which was verified by qRT-PCR and *in situ* hybridization. Furthermore, we observed an expression switch of two *Myl6* isoforms after mechanical stretch. This switch is accompanied by a change in a C-terminally located amino acid sequence.

In summary, mechanical stretch of cultured podocytes is an excellent model to simulate hypertensive nephropathy. In depth RNA-Seq analysis disclosed alternative splicing events, such as in *Shroom3* and *Myl6*, which may play a crucial role in the pathophysiology of hypertension-induced nephropathy.

Introduction

The podocytes, highly differentiated visceral epithelial cells in the kidney glomerulus, play a crucial role in the maintenance of the glomerular filtration barrier. Hypertension is a contributing factor to the progression of chronic kidney disease (CKD) and the development of end-stage kidney disease (ESKD).[1,2] Hypertensive nephropathy (HN) is caused by high blood pressure and the instability of podocyte architecture, resulting from the effacement of podocyte foot processes (FPs) or podocyte detachment.[3] As mature podocytes have limited ability to divide, damaged or lost podocytes cannot be replaced.[4,5]

In higher eukaryotes, alternative splicing (AS) is the main process for generating transcriptome and proteome diversity for tissue- and development-specific expression. It has been shown that pre-mRNAs from approximately 95% of human genes with multiple exons undergo AS, resulting in multiple protein isoforms with different structures and functions from a single gene.[6]

Several studies have shown that defects in AS regulation may be the initial trigger for various diseases, including cancer,[7-9] cardiovascular diseases,[10] neurodegenerative diseases,[11,12] and neuromuscular diseases.[13] Since the completion of the sequencing and annotation of the human genome, several next-generation sequencing techniques have become available. As a result, the number of diseases found to be associated with changes in alternative splicing has increased dramatically.

Previous studies have described individual AS events that affect the development of kidney injuries. For instance, intron retention and the presence of an early stop codon result in the production of soluble Klotho (sKlotho).[14,15] Supplementation of sKlotho has demonstrated a nephroprotective effect in model animals with CDK.[16,17] During the early stages of diabetic nephropathy (DN), the mRNA level of the VEGF-A_{165}b splice isoform (vascular endothelial growth factor) increases to protect the glomerular filtration barrier.[18] The podocyte-specific protein WT1 also has two characteristic splicing events: the inclusion or skipping of exon 5 and the alternative use of two splice donor sites between exons 9 and 10, leading to the expression of two major protein isoforms, WT1(+KTS) and WT1(-KTS).[19] Mice lacking the WT1(-KTS) variant exhibit more severe kidney defects, while those lacking the WT1(+KTS) variant show disturbed podocyte function.[20]

However, no studies have yet been reported in the literature on the correlation between AS defects and HN. In this study, we used our *in vitro* hypertension mouse model[21] to compare omics data, detect and quantify AS events, gene isoforms, and isoform switches in mechanically stretched podocytes. In this context, we identified several significantly alternatively spliced transcripts, and focused on Myl6 (Myosin light chain 6) and Shroom3 (Shroom family member 3). Myl6, a cellular motor protein that generates force for cellular

movements, is highly expressed in podocytes. Genome-wide association studies have found that SNPs in SHROOM3 are associated with chronic kidney disease (CKD) and lower estimated Glomerular Filtration Rate (eGFR).[22-26] Additionally, Shroom3 deficiency in mice leads to glomerular abnormalities, albuminuria, and changes in podocyte morphology, such as foot process effacement.[27,28]

In summary, we detected differential AS events that may contribute to the development of hypertension-related glomerulopathies. These findings identify potential biomarkers that could be useful in predicting the onset and progression of these diseases.

Methods

Cell Culture

Conditionally immortalized podocytes (SVI; CLS Cell Line Service GmbH, Eppelheim, Germany) were handled as described previously.[21] Briefly, podocytes were maintained in RPMI 1640 medium (Sigma-Aldrich, St. Louis, MO, USA) supplemented with 10% fetal bovine serum (FBS; Boehringer Mannheim, Mannheim, Germany), 100 U/ml penicillin, and 0.1 mg/ml streptomycin (Thermo Fisher Scientific, Waltham, MA, USA). To propagate podocytes, we cultivated cells at 33°C. To induce differentiation, we maintained podocytes at 38°C for at least two weeks before applying mechanical stress.

Mechanical stretch experiments

Mechanical stretch experiments were performed according to our previous study.[21] Differentiated mouse podocytes were seeded on flexible silicon membranes of a six well plate (Bioflex, Flexcell® International Corporation, Burlington, NC, USA). The flexible silicone membranes were coated with collagen IV to facilitate cell attachment. After 3 days, the six well plate was mounted on a manifold connected to a custom-built stretch apparatus (NIPOKA GmbH, Greifswald, Germany), which induced cyclic variations in air pressure below and above atmospheric pressure. Cyclic pressure variations caused upward and downward motion of the silicone membranes. Pressure amplitude was chosen to give a maximum up- and downward deflection of the membrane center of 6 mm (low stretch), being equal to an increase in membrane area by 11%, or 5% mean linear cell strain. For the high stretch experiments, experiments were performed with a higher amplitude (8 mm). Cycle frequency was adjusted to 1 Hz. This frequency was chosen because autoregulation of renal blood flow is capable of damping pressure fluctuations below 0.1 Hz, whereas faster pressure fluctuations (> 0.1 Hz) are fully transmitted to glomerular capillaries.[29,30] Number of adherent cells was determined by counting stained podocytes from at least three biological replicates.

Ang II-induced hypertensive mice

Induction of Ang II-induced hypertension has been described previously.[31,32]

Isolation of murine glomeruli

To analyze individual glomeruli, the kidneys were removed, and chopped up with scissors with 1 ml of cold Hank's Balanced Salt Solution (HBSS; Thermo Fisher Scientific). The cell suspension was then centrifuged at 300 × g for 5 min at 4°C. The supernatant was discarded, the cell pellet was digested with 1 ml of collagenase A (5 mg/ml) (Roche, Basel, Switzerland) and washed with 3 ml cold HBSS at 37°C for 15 min with gentle agitation. The reaction was

stopped with 4 ml of RPMI 1640 (Sigma-Aldrich) without phenol supplemented with 10% fetal bovine serum (Thermo Fisher Scientific).

The digested tissue was spun down at 300x g for 5 min at 24°C, the supernatant was discarded and the pellet was dissolved in 1 ml of HBSS. The digested tissue was then gently pressed through a 150 µm cell strainer (pluriSelect, Leipzig, Germany) and large tissue particles were pressed through the strainer with the rubber plunger of a 1-ml syringe. The procedure was repeated with cell strainers of different diameters (100 µm and 40 µm). The glomerular and tubular fragments are retained above 40 µm. The supernatant containing highly purified glomeruli was collected and centrifuged at 300x g at 24°C for 5 min. The supernatant was then removed and in 1 ml Tri-Reagent (Sigma-Aldrich) was added.

RNA extraction, cDNA synthesis and qRT-PCR

Cells were processed in Tri-Reagent (Sigma-Aldrich) according to manufacturer's instructions. For cDNA synthesis, 1 µg of the isolated total RNA was transcribed using the QuantiTect Reverse Transcription Kit (Qiagen, Hilden, Germany). The quantitative real-time PCR (qRT-PCR) analysis was performed on a Bio-Rad iQ5 (Bio-Rad, Hercules, CA, USA) using the iTaq Universal SYBR Green Supermix (Bio-Rad) with *Gapdh* as reference gene. Relative quantifications of the mRNA levels were done by the efficiency corrected calculation model by Pfaffl[33] and are shown with standard deviations (SD) or standard error of the mean (SEM) from at least three biological replicates.

Liquid chromatography-mass spectrometry (LC-MS)

Mechanically low and high stretched podocytes of three independent bioreplicates were harvested in Trizol and treated according to manufacturer’s protocol. Protein was obtained from the corresponding phase by isopropanol precipitation. Protein pellet was reconstituted in Tris-HCl (10 mM, pH 7.5) with 5% SDS. Protein concentration was determined by BCA assay (Pierce/Thermo Fisher Scientific). We used an adapted bead based SP3 protocol[34] for removal of contaminants and proteolytic digestion. Briefly, five µg protein were reduced by 2.5 mM dithiothreitol for 30 min at 37°C and alkylated with 10 mM iodoacetic acid for 30 min at 37°C in the dark before digestion by trypsin (Promega, Walldorf, Germany) in a protein to enzyme ratio 25:1 overnight at 37°C. Peptides were separated by LC (Ultimate 3000, Thermo Electron, Bremen, Germany) before data-independent acquisition of MS data on an Exploris 480 mass spectrometer (Thermo Electron). MS data were analyzed via the DirectDIA algorithm implemented in Spectronaut (v17, Biognosys, Zurich, Switzerland) using an Uniprot database (version 2021_2) limited to *Mus musculus* (n=17063). Carbamidomethylation at cysteine was set as static modification, oxidation at methionine and protein N-terminal acetylation were defined as variable modifications, and up to two missed cleavages were allowed. Proteins were

only considered for further analyses, if two or more unique+razor peptides were identified and quantified per protein. Data were median normalized on ion level before statistical analysis was carried out on peptide level after exclusion of peptides with oxidized methionine using the algorithm ROPECA.[35] Binary differences were identified by application of a reproducibility-optimized test statistic (using the ROTS package). Only proteins that showed different abundance (p-value < 0.05) were used for further considerations.

RNA-seq and AS event analysis

RNA-Seq raw reads for low-stretch, high-stretch, and unstretched podocytes were mapped to the mouse reference genome mm39 with the genome annotation from Ensembl version 104 using STAR version 2.7.5c.[36] We used the default parameters with a 2-pass mode recommended for alternative splicing analysis. Gene read counts were obtained by the featureCounts tool included in the Subread 2.0.0.[37] Read counts were further normalized and used for differential gene expression by DESeq2 version 1.38.3.[38] For isoform switch analysis, we prepared transcript counts using salmon version 1.9.0[39] with the transcript annotation based on Ensembl version 104 and ran the R package IsoformSwitchAnalyzeR version 1.20.0[40] with the DESeq2 algorithm. For alternative splicing analysis, we used MAJIQ version 2.3,[41] leafcutter version 0.2.9,[42] rMATS version 4.1.2, and Whippet version 0.11.1 (with julia 1.6.6)[43] with the default parameters. We defined significantly differentially used events as events with a p-value < 0.05 (for leafcutter, rMATS, and Whippet) or a confidence > 0.95 (for MAJIQ).

Immunofluorescence staining

Cells were fixed using 2% PFA (paraformaldehyde) in PBS (phosphate buffered saline) for 10 min at room temperature (RT), washed and subjected to blocking solution (PBS, 2% fetal bovine serum, 2% bovine serum fraction V, 0.2% fish gelatine) for 1 hour at RT. Primary antibodies were incubated for 60 min at RT. Actin was stained using Alexa Fluor® phalloidin (Thermo Fisher Scientific). After a washing step with PBS (3 × 3 min) cells were incubated with secondary antibodies for 40 min at RT. Bound antibodies were visualized with Cy2- or Cy3-conjugated secondary antibodies (Jackson ImmunoResearch Laboratories, West Grove, USA). For nuclei staining DAPI (Sigma-Aldrich, 1 µg/ml) was used for 5 min. All samples were mounted in Mowiol (Carl Roth, Karlsruhe, Germany) and used for laser scanning microscopy (LSM). For paraffin sections, samples were dehydrated and embedded in paraffin by standard procedures. Paraffin sections (5 µm) were cut on a Leica SM 2000R (Leica Microsystems, Wetzlar, Germany). After rehydration, sections were unmasked in Tris (pH 9.0) or in citrate buffer (0.1 M, pH 6.0) by heating for 5 min in a pressure cooker. The sections were stained with 1 µg/ml DAPI (Sigma-Aldrich) for 5 min. For immunofluorescence double-staining,

samples were incubated with an antibody against MYL6 (PA5-106803; from Thermo Fisher Scientific) and synaptopodin (61094, Progen Biotechnik GmbH, Heidelberg, Germany) overnight. Samples were washed with 1x PBS for 3x5 min and incubated with Cy2- and Cy3-conjugated secondary antibodies (Jackson ImmunoResearch Laboratories) for 1 hour. After additional washing, the samples were mounted in Mowiol (Carl Roth) for fluorescence microscopy.

Histology on human kidney biopsies

Kidney biopsies were received from the Department of Nephropathology, Institute of Pathology, University Hospital Erlangen, Germany. The use of remnant kidney biopsy material was approved by the Ethics Committee of the Friedrich-Alexander-University of Erlangen-Nuremberg, waiving the need for retrospective consent for the use of archived rest material (Re.-No.4415 and Re.-No.22-150-D). Sample fixation and preparation of the control, HN, DN, and FSGS group were identical.

Combined multiplex fluorescence *in situ* hybridization (RNAscope) and immunofluorescence

RNA *in situ* hybridization was performed for Shroom3 isoforms using RNAscope Multiplex Fluorescent V2 kit (Advanced Cell Diagnostics, Inc.) with the following modifications. Tissue sections were deparaffinized in xylene (two times for 5 min) and rehydrated in 100% ethanol (two times for one minute). The pre-treatment procedure included the application of RNAscope Hydrogen Peroxide (10 min at room temperature), the submersion in boiling RNAscope Target Retrieval reagent (15 min), and the treatment with RNAscope Protease Plus (15 min at 40°). RNA scope complementary probes were hybridized for 2 hours at 40°C in the ACDbio HybEZ oven. Each probe has been assigned a different channel: Shroom3_054 (Cat No. 1276721-C1), Shroom3_055 (Cat No. 1077361-C2) and Shroom3_438 (Cat No. 1298351-C3). 3-plex Positive (Polr2a, Ppib and Ubc) and 3-plex Negative Control (dapB) probes were used as positive control and negative control, respectively. Sections were stored in 5× SSC (Invitrogen) overnight. The hybridization signals were then amplified and detected using Opal 520, 570 and 690 dyes diluted 1:1500 in TSA amplification buffer (ACDbio). After the detection steps, sections were subjected to blocking solution (PBS, 2% fetal bovine serum, 2% bovine serum fraction V, 0.2% fish gelatine) for 1 hour at RT (room temperature) and incubated with primary antibody against podocin (1:150) (IBL International GmbH, Hamburg, Germany). Primary NPHS2 antibodies were detected using AlexaFluor 750 secondary antibodies. Slides were counterstained with DAPI (Sigma-Aldrich, 1 µg/ml) and mounted in Mowiol (Carl Roth) and imaged by confocal laser scanning microscopy.

Laser scanning microscopy

Images were captured with an Olympus FV3000 confocal microscope (Olympus, Tokyo, Japan) with 20x/40x/60x oil immersion objectives and Olympus FV3000 CellSense software.

Statistical and bioinformatic analysis

Data were analysed by Gene Set Enrichment Analysis (GSEA) and the use of QIAGEN IPA (QIAGEN Inc.). For the analysis of the differentially abundant proteins and transcripts R scripts including the libraries EnhancedVolcano and ComplexHeatmap were used for the visualization. The heatmaps include on the Y-axis a dendrogram of the hierarchical clustering after z-score normalization of the protein abundance values in the different samples. The heatmaps are used to represent the abundance of proteins as ratio from treatment versus control of specific biological pathways from the GeneOntology (GO). To detect the enriched or overrepresented pathways and their protein protein interactions the cnetplots and dotplots from the GO biological processes were created using the library clusterProfiler.[44]

The GraphPad Prism 9 software was used for statistical analysis of experimental data and preparation of graphs. Scatter plots indicate individual units used for statistical testing (samples, cells or replicates), as specified in respective figure legends. Data are given as means ±SD or ±SEM, analyzed by unpaired *t* test with repeated measurements (n). For multiple groups statistical analyses were done by ANOVA with a Benjamini-Hochberg post-hoc test. Statistical significance was defined as $p < 0.05$ and significance levels are indicated as * $p < 0.05$, ** $p < 0.01$, *** $p < 0.001$, **** $p < 0.0001$ and non-significant (ns) in respective figure panels. The number of independent experiments and analyzed units are stated in the figure legends.

Results

Proteomics and transcriptomics of mechanically stretched podocytes

To determine whether mechanical stretch regulates alternative splicing, podocytes were cultured on flexible silicone membranes and stretched at low or high stretch conditions for three days (Fig. 1A). The mRNA and proteins were isolated and analyzed using complementary transcriptome (RNA-Seq) and proteome analysis (LC-MS/MS) (Fig. 1B).

Proteome analysis revealed significant alterations upon mechanical stretch. A total of 135 proteins showed different levels under low stretch conditions (54 increased and 81 decreased). Under high stretch conditions, 424 proteins were altered (195 increased and 229 decreased) compared to the unstretched condition (cutoffs: adj. p-value < 0.05 and fold change ≥ 1.5) (Fig. 1C-D). These results show that higher mechanical stress leads to a strong regulation of proteins in podocytes. From 787 differentially abundant proteins (cutoff: adj. p-value < 0.05), 157 (20%) are found in both low and high stretch conditions (Fig. 1E).

We further show that there is no significant difference in the protein levels using mono-axial or bi-axial extension of the stretch membrane (Fig. S1). Gene set enrichment analysis (GSEA) for gene ontology (GO) terms revealed an up-regulation of proteins associated with mRNA processing and RNA splicing (Fig. 1F-G and Fig. S2A). In contrast, the majority of proteins with decreased intensity upon stretch were cytoskeleton and actin-binding proteins (Fig. 1H-I and Fig. S2B). GSEA from low stretched podocytes showed a comparable enrichment of GO-Terms (Fig. S2C-F).

Transcriptome analyses using RNA sequencing confirmed that increased mechanical stress results in a higher number of differentially expressed genes. We observed 20% more down- and 106% more significantly up-regulated genes under high stretch conditions, compared to low stretch conditions (Fig. 2A-B). In total, we identified more than 1300 significantly regulated genes after mechanical stretch compared to unstretched podocytes (Fig. 2C). The GSEA of the transcriptome showed a similar enrichment of GO-Terms compared to the proteome (Fig. S3). Notably, several of the regulated targets are long non-coding RNAs (lncRNAs), that might impact gene regulation (Fig. 2C).

We further investigated which proteins are differentially regulated at the RNA as well as at the protein level. Our analysis identified 25 targets that were significantly regulated under both low and high stretch conditions on transcript as well as on protein level (Fig. 2D-E). Changes in the abundance of proteins and RNA were significantly higher at high stretch conditions in comparison to low stretch conditions. For example, the extracellular matrix protein fibronectin, which is essential for podocyte adhesion,[45] was found to be expressed 1.6-fold (at the RNA

level) and even 3.2-fold (at the protein level) higher under high stretch conditions than under low stretch conditions (Fig. 2E). Furthermore, other known podocyte injury markers, such as Serpine1 or ezrin, were also significantly regulated at the mRNA and protein level, confirming mechanical stretch as a model for hypertension.

The regulation of the expression of various candidates was verified by qRT-PCR (Fig. S4). Interestingly, most of the genes/proteins that were regulated in our *in vitro* hypertension model were also significantly regulated *in vivo* in patients with diabetic nephropathy (DN), which is often associated with glomerular hypertension, or in DN mice (Fig. 3E).

Alternative splicing in mechanically stretched podocytes

To identify alternative splicing (AS) events, we used several AS tools (Leafcutter, MAJIQ, rMATS and WHIPPET). Additionally, we analyzed isoform switches using IsoformSwitchAnalyzeR[40] (Fig. 3A). We found a wide variety of splicing events. The most frequent event was exon skipping (between 63-82% of all AS events), followed by intron retention and alternative 5′ or 3′ splice sites (Fig. 3B). We detected 290 alternative spliced genes detected using three different splice analysis tools (Fig. 3C). Of these 290 genes, 17 candidates also showed a significant isoform switch, including *Abca3*, *Arhgap22*, *Cenpi*, *Ikbkg*, *Myl6*, *Os9*, *Pja2*, *Prrc2b*, *Rgs12*, *Rps24*, *Rusc2*, *Shroom3*, *Slc27a1*, *Snx14*, *Sptan1*, *Tnnt2* and *Zfp219* (Fig. 3C-F, Fig. S5). To prioritize, we examined the renal and glomerular expression of these genes (Fig. 3D-E; Fig. S6). Furthermore, we screened which candidates were also present in the proteome, suggesting a podocyte-specific expression, and which showed a glomerular upregulation *in vivo* under hypertensive conditions (Fig. 3F). Based on these criteria, we initially focused on Myl6 and Shroom3.

Myl6 is alternative spliced in mechanically stretched podocytes

Myosin light chain 6 (Myl6), a component of the myosin motor protein complex, is highly expressed in cultured *in vitro* and *in vivo* podocytes (Fig. 4A-B and Fig. S9). RNA-Seq data confirmed that *Myl6* is the most expressed myosin in podocytes (43 % of all myosins), which shows the importance of MYL6 for podocytes. (Fig. 4C). However, the *Myl6* expression is slightly, but not significantly increased after mechanical stretch (Fig. 4D). Furthermore, we have not observed a significant change of the MYL6 level in patients with hypertensive or diabetic nephropathy (Fig. 4E).

We further studied the expression of isoforms of *Myl6*. We were able to detect two isoforms (Fig. 4F), which were differentially expressed in stretched versus unstretched conditions (Fig. 4H-J). However, the basic expression of both isoforms is almost identical *in vitro* (Fig. 4I)

and *in vivo* (Fig. 4K). The two isoforms have the same length but differ in their C-termini (Fig. 4F-G). Isoform 2 (ENSMUST00000218127/NM_001317218) contains an alternate exon in the 3' coding region, resulting in a frameshift and a novel 3' UTR. This results in an amino acid switch from ELVRMVLN to AFVRHILS (Fig. 4L). These motifs are well conserved in mice, rats, and humans (Fig. 4M). Using the protein structure analysis tool StructMAn[46] on these Myl6 isoforms, it was found that this amino acid substitution affects the actin binding domain (ABD) and weakens the actin interaction surface (Fig. 4N). Therefore, the isoform that increases after mechanical stretch has a higher potential for interaction with actin, which could benefit in withstanding increased mechanical stress.

Alternative splicing of *Shroom3 in vitro* and *in vivo*

The National Center for Biotechnology Information (NCBI) database describes four different *Shroom3* transcripts (https://www.ncbi.nlm.nih.gov/gene/27428). All transcripts were identified in our cultured murine podocytes by RNA-Seq (Fig. 5A), with varying expression levels (Fig. 5C). Surprisingly, mouse podocytes express protein isoform 1 (encoded by ENSMUST00000113055) at a very low level. This isoform is the longest and the only transcript that includes the PDZ domain and in human the intron with a GFR-associated SNP (Fig. 5A-B, Fig. S7). The transcript ENSMUST00000113054 (NM_001077595) encodes protein isoform 2, which has the same protein sequence like transcript variant ENSMUST00000113051, but differs in the 5' UTR (Fig. 5A-B, S7). The isoform ENSMUST00000113054 was expressed at the highest level of all isoforms and showed a significant decrease in expression after mechanical stretch (Fig. 5C, E). Isoform ENSMUST00000225438 (XM_006534966) was up-regulated after mechanical stretch (Fig. 5C-E). Downstream analysis by IsoformSwitchAnalyzeR showed for both isoforms a significantly changed usage after mechanical stretch (Fig. 5D), which was confirmed by qRT-PCR (Fig. 5E). By qRT-PCR of murine glomeruli, we could also impressively show that the *Shroom3* isoform ENSMUST00000113054 is the dominant renal glomerular *Shroom3* isoform *in vivo* (16-fold higher expressed than ENSMUST00000225438) (Fig. 5F). This was confirmed by *in situ* hybridization experiments (Fig. 5I and Fig. S8). Additionally, *Shroom3* isoform ENSMUST00000113054 is exclusively expressed in the renal glomerulus (Fig. 5G). This finding was quantified with qRT-PCR, which showed that *Shroom3* ENSMUST00000113054 was around 12-fold enriched in isolated glomeruli in comparison with total kidney fractions (Fig. 5G). In a published isolated podocyte versus bulk glomerulus mass spectrometry dataset, podocyte-specificity of SHROOM3 in comparison to whole glomeruli could be verified (Fig. 5H).

To find out whether *Shroom3* is also regulated in mice suffering from hypertension, we analyzed the mRNA expression of *Shroom3* in murine kidneys with angiotensin II-induced hypertension (Fig. 5J). We observed that hypertensive mice showed a significant increase of *Shroom3* mRNA compared to the control mice (Fig. 5J). Furthermore, in human CKD patients and in our dedifferentiation GlomAssay, we observed a significant up-regulation of SHROOM3 (Fig. 5K and L).

To study the importance of *Shroom3* for podocytes, *Shroom3* was knocked down in cultured mouse podocytes using specific siRNA. Knockdown efficiency was validated by qRT-PCR (Fig. S9). After treatment with specific siRNA against *Shroom3*, we observed a reorganization of the actin fibers specifically in *Shroom3* knockdown podocytes (*Shroom3* KD) (Fig. 5M). In contrast, we found mostly transversal stress fibers in the control cells as measured with the OrientationJ plugin[47] for ImageJ (Fig. 5M). The relative coherence of the analyzed actin fibers was significantly reduced by 28% in *Shroom3* KD podocytes compared to the control (Fig. 5N). Interestingly, the total mRNA amount of actin (*Actb*) was significantly higher in *Shroom3* KD podocytes compared to the Ctrl (Fig. S10B). In contrast, the expression of intermediate filament and microtubule markers was not affected by *Shroom3* KD (Fig. 10B). Furthermore, we observed that with increasing siRNA concentration and the associated stronger knockdown effect, there is a dramatic reduction in F-actin formation (Fig. 5O-P and Fig. S10D). The proportion of cells without (visible) F-actin increased to over 70% at higher siRNA concentration. In contrast, the control cells transfected with the same concentration of negative scrambled siRNA do not show a higher proportion of cells without visible F-actin (Fig. 5P and Fig. S10D). The loss of SHROOM3 appears to result in an impaired polymerization of G-actin monomers to F-actin.

Discussion

Podocyte damage and detachment caused by mechanical stress is a common issue in hypertension-induced glomerular disease.[21,48] One of the cellular mechanisms that allow podocytes to adapt to these conditions is alternative splicing, a process that enables a single gene to produce multiple protein isoforms with distinct functions.[49,50] This process is particularly important in podocytes, as they must dynamically reorganize their cytoskeleton, which is essential for maintaining podocyte structure and function, in response to mechanical stress, such as increased glomerular pressure in hypertension.

Our initial findings demonstrated that our *in vitro* hypertension model accurately reflects podocyte stress conditions. The mechanically stretched podocytes exhibited significant regulation of numerous known podocyte injury markers, including fibronectin, serpine1, and ezrin.[45,51-54] These proteins serve as important markers of podocyte stress, reflecting the cellular response to mechanical stress, such as increased glomerular pressure due to hypertension. Their regulation is associated with processes such as fibrosis or extracellular matrix and cytoskeleton remodeling, which are key features of chronic kidney disease and hypertensive nephropathy. Understanding the roles and regulatory mechanisms of these proteins in podocytes can provide valuable insights into the pathophysiology of kidney diseases and identify potential targets for therapeutic intervention.

Furthermore, our findings indicate that advanced mechanical stress results in more significantly regulated proteins. This observation is consistent with the established correlation between elevated blood pressure levels and pronounced glomerular alterations.[55-57] Among the regulated proteins were numerous proteins with a function in RNA splicing, such as YB-1, which is translocated into the nucleus for transcriptional regulation under cellular stress conditions, including cold shock and oxidative stress.[58,59] This demonstrates the potential significance of alternative splicing for the adaptation of podocytes to mechanical stress.

In podocytes, alternative splicing seems to affect several key genes involved in cytoskeletal dynamics, cell signaling, and adhesion. For instance, the alternative splicing of nephrin, a critical slit diaphragm protein, can influence its interaction with other podocyte proteins and the structural integrity of the filtration barrier.[60,61] Similarly, splicing variations in the WT1 gene, a well-known regulator of podocyte differentiation, produce different isoforms that can modulate gene expression patterns crucial for podocyte differentiation and stress.[62-64]

In the present study, we have identified numerous novel genes that undergo alternative splicing in response to mechanical stretch. The most prevalent AS event identified in our study was exon skipping, a finding that is supported by data from Sugnet *et al.*.[65]

A comprehensive analysis of alternative splicing was conducted to assess the relative strengths and limitations of various computational systems, including rMATS, MAJIQ, leafcutter, and Whippet. Some models demonstrated high precision and robustness in identifying splicing events, particularly in the presence of biological replicates. Conversely, others were designed to discover new events without the need for pre-defined reference annotations.[42,43,66] A common limitation of rMATS, leafcutter, and Whippet is that they are unable to detect isoforms with opposite regulation. Consequently, the IsoformSwitchAnalyzeR algorithm was also used for that reason.[40]

The robustness of our findings is evidenced by the observation that our most promising candidates (Myl6 and Shroom3) were identified as alternatively spliced in all utilized AS tools. Furthermore, both are expressed in podocytes and showed a significant isoform switch after mechanical stretch.

MYL6, being part of the actin-myosin complex, contributes to the organization and function of the actin cytoskeleton in podocytes, which is critical for maintaining the structural integrity of podocytes. In podocytes, the expression of *Myl6* is markedly high; this could indicate that *Myl6* plays an important role in the adaptation of cells to mechanical stress and in the reorganization of cell structure under pathological conditions such as hypertension. By single-cell RNA sequencing and RNA FISH, the group of J. Salzman detected *Myl6* spliced isoforms in murine smooth muscle cells and human lung.[67] To the best of our knowledge, we are the first to detect the existence of two distinct alternatively spliced Myl6 isoforms in podocytes. In glomerular diseases that damage podocytes, such as hypertensive nephropathy, dysregulation of *Myl6* splicing may impair the ability of podocytes to maintain their structure and function.

SHROOM3 is a crucial protein in podocytes and is involved in maintaining the cytoskeletal architecture of podocytes.[27] Furthermore, genome-wide association studies have found that SNPs in *SHROOM3* are associated with chronic kidney disease (CKD) and lower estimated Glomerular Filtration Rate (eGFR).[22-26] It interacts with actin filaments to regulate cell shape and adhesion, ensuring that podocytes can withstand the mechanical stress. Disruption in *Shroom3* expression or function can lead to cytoskeletal disorganization, resulting in podocyte effacement and proteinuria, a hallmark of glomerular diseases.[28] Our study represents the inaugural investigation to demonstrate that specific *Shroom3* transcript isoforms are exclusively expressed in podocytes and that their expression levels undergo significant alterations in various injury models. This knowledge could be used to utilize specific *Shroom3* isoforms as splicing biomarkers for the diagnosis of patients with hypertensive nephropathy. The importance of *Shroom3* for podocytes was impressively demonstrated by knockdown experiments, which showed the essential role of *Shroom3* for the stability and maintenance of the actin cytoskeleton in podocytes. The loss of *Shroom3* appears to result in an impaired

polymerization of G-actin monomers to F-actin. This finding is consistent with previous reports indicating that all Shroom family proteins interact with actin and are essential for actin polymerization.[68]

It is noteworthy that there is a link between SHROOM3 and MYL6 (as part of the essential light chain of myosin II).[69-71] It is known that the ASD2 domain of Shroom3 can bind directly to Rho-associated kinases (ROCKs).[72-74] Once ROCKs are activated by RhoA, they phosphorylate the myosin regulatory light chain to activate myosin II, resulting in F-actin contraction.[73,75-78] This molecular pathway is supported by studies demonstrating that Shroom3 colocalizes with actin filaments, RhoA, ROCKs, and myosin II at adherens junctions.[73,79,80] In Shroom3 homozygous null mutant mice podocytes, a reduced ROCK1 expression and phosphorylation was observed, which further confirmed that Shroom3 regulates the actomyosin cytoskeleton through the ROCK/Myosin II signaling pathways.[27]

In summary, understanding the role of alternative splicing in podocyte biology offers potential therapeutic avenues for hypertensive nephropathy. Targeting pathways involved in the regulation of critical podocyte genes, such as *Shroom3* and *Myl6*, could help restore normal splicing patterns and improve podocyte function. Small molecules or antisense oligonucleotides that modulate splicing could correct mis-splicing events and enhance podocyte resilience to hypertensive stress. Moreover, *Myl6* or *Shroom3* may serve as splicing biomarkers associated with hypertensive nephropathy, offering the potential for early diagnosis and personalized treatment strategies.

Author Contributions Statement

The study was designed by K.E., N.E. and F.K.; F.K., F.M. contributed to the cell culture experiments; biopsies were handled and analyzed by K.A., F.K., F.M.; LC-MS/MS was performed by E.H. and U.V.; RNA-Seq was performed and analyzed by O.T. and C.L.; protein structure analysis were done by A.G. and O.K., mice experiments were performed by U.W., F.M.; all other experiments were performed by F.K. and F.M.; experimental data were analyzed by F.K., F.M., O.T., S.A., S.S., C.L.; F.K., F.M. and N.E. wrote the main manuscript text. F.K. and F.M. prepared figures. All authors reviewed the manuscript.

Data availability

All data supporting the findings of this study are available within the paper. All other relevant data and materials are available from the corresponding author on reasonable request.

Disclosure Statements

The authors declare no competing interests.

The authors declare no competing financial interests.

The authors confirm that there are no conflicts of interest.

References

1. Bidani AK, Griffin KA. Pathophysiology of hypertensive renal damage: implications for therapy. *Hypertension*. 2004;44(5):595-601. doi:10.1161/01.HYP.0000145180.38707.84
2. Wiggins RC. The spectrum of podocytopathies: a unifying view of glomerular diseases. *Kidney Int*. 2007;71(12):1205-1214. doi:10.1038/sj.ki.5002222
3. Kriz W, Gretz N, Lemley KV. Progression of glomerular diseases: is the podocyte the culprit? *Kidney Int*. 1998;54(3):687-697. doi:10.1046/j.1523-1755.1998.00044.x
4. Lasagni L, Lazzeri E, Shankland SJ, Anders H-J, Romagnani P. Podocyte mitosis - a catastrophe. *Curr Mol Med*. 2013;13(1):13-23. doi:10.2174/1566524011307010013
5. Mulay SR, Thomasova D, Ryu M, et al. Podocyte loss involves MDM2-driven mitotic catastrophe. *J Pathol*. 2013;230(3):322-335. doi:10.1002/path.4193
6. Pan Q, Shai O, Lee LJ, Frey BJ, Blencowe BJ. Deep surveying of alternative splicing complexity in the human transcriptome by high-throughput sequencing. *Nat Genet*. 2008;40(12):1413-1415. doi:10.1038/ng.259
7. Strnad L, Kruparzh V, Ulybin B. Metody otsenki effektivnosti diagnosticheskikh podkhodov. *Sb Ved Pr Lek Fak Karlovy Univerzity Hradci Kralove*. 1989;32(1):9-29.
8. Zhang Y, Wu X, Li J, et al. Comprehensive characterization of alternative splicing in renal cell carcinoma. *Brief Bioinform*. 2021;22(5). doi:10.1093/bib/bbab084
9. Biernacka KM, Barker R, Sewell A, Bahl A, Perks CM. A role for androgen receptor variant 7 in sensitivity to therapy: Involvement of IGFBP-2 and FOXA1. *Transl Oncol*. 2023;34:101698. doi:10.1016/j.tranon.2023.101698
10. Schoenauer R, Emmert MY, Felley A, et al. EH-myomesin splice isoform is a novel marker for dilated cardiomyopathy. *Basic Res Cardiol*. 2011;106(2):233-247. doi:10.1007/s00395-010-0131-2
11. Heinzen EL, Yoon W, Weale ME, et al. Alternative ion channel splicing in mesial temporal lobe epilepsy and Alzheimer's disease. *Genome Biol*. 2007;8(3):R32. doi:10.1186/gb-2007-8-3-r32
12. Elliott DA, Kim WS, Gorissen S, Halliday GM, Kwok JBJ. Leucine-rich repeat kinase 2 and alternative splicing in Parkinson's disease. *Mov Disord*. 2012;27(8):1004-1011. doi:10.1002/mds.25005
13. Zhang Z, Lotti F, Dittmar K, et al. SMN deficiency causes tissue-specific perturbations in the repertoire of snRNAs and widespread defects in splicing. *Cell*. 2008;133(4):585-600. doi:10.1016/j.cell.2008.03.031
14. Matsumura Y, Aizawa H, Shiraki-Iida T, Nagai R, Kuro-o M, Nabeshima Y. Identification of the human klotho gene and its two transcripts encoding membrane and secreted klotho protein. *Biochem Biophys Res Commun*. 1998;242(3):626-630. doi:10.1006/bbrc.1997.8019
15. Shiraki-Iida T, Aizawa H, Matsumura Y, et al. Structure of the mouse klotho gene and its two transcripts encoding membrane and secreted protein. *FEBS Lett*. 1998;424(1-2):6-10. doi:10.1016/s0014-5793(98)00127-6
16. Haruna Y, Kashihara N, Satoh M, et al. Amelioration of progressive renal injury by genetic manipulation of Klotho gene. *Proc Natl Acad Sci U S A*. 2007;104(7):2331-2336. doi:10.1073/pnas.0611079104
17. Hu MC, Kuro-o M, Moe OW. Secreted klotho and chronic kidney disease. *Adv Exp Med Biol*. 2012;728:126-157. doi:10.1007/978-1-4614-0887-1_9
18. Bevan HS, van den Akker NMS, Qiu Y, et al. The alternatively spliced anti-angiogenic family of VEGF isoforms VEGFxxxb in human kidney development. *Nephron Physiol*. 2008;110(4):p57-67. doi:10.1159/000177614
19. Bor Y, Swartz J, Morrison A, Rekosh D, Ladomery M, Hammarskjöld M-L. The Wilms' tumor 1 (WT1) gene (+KTS isoform) functions with a CTE to enhance translation from an unspliced RNA with a retained intron. *Genes Dev*. 2006;20(12):1597-1608. doi:10.1101/gad.1402306

20. Wagner K-D, Wagner N, Schedl A. The complex life of WT1. *J Cell Sci*. 2003;116(Pt 9):1653-1658. doi:10.1242/jcs.00405
21. Endlich N, Kress KR, Reiser J, et al. Podocytes respond to mechanical stress in vitro. *J Am Soc Nephrol*. 2001;12(3):413-422. doi:10.1681/ASN.V123413
22. Köttgen A, Glazer NL, Dehghan A, et al. Multiple loci associated with indices of renal function and chronic kidney disease. *Nat Genet*. 2009;41(6):712-717. doi:10.1038/ng.377
23. Ellis JW, Chen M-H, Foster MC, et al. Validated SNPs for eGFR and their associations with albuminuria. *Hum Mol Genet*. 2012;21(14):3293-3298. doi:10.1093/hmg/dds138
24. Yeo NC, O'Meara CC, Bonomo JA, et al. Shroom3 contributes to the maintenance of the glomerular filtration barrier integrity. *Genome Res*. 2015;25(1):57-65. doi:10.1101/gr.182881.114
25. Prokop JW, Yeo NC, Ottmann C, et al. Characterization of Coding/Noncoding Variants for SHROOM3 in Patients with CKD. *J Am Soc Nephrol*. 2018;29(5):1525-1535. doi:10.1681/ASN.2017080856
26. Wuttke M, Li Y, Li M, et al. A catalog of genetic loci associated with kidney function from analyses of a million individuals. *Nat Genet*. 2019;51(6):957-972. doi:10.1038/s41588-019-0407-x
27. Khalili H, Sull A, Sarin S, et al. Developmental Origins for Kidney Disease Due to Shroom3 Deficiency. *J Am Soc Nephrol*. 2016;27(10):2965-2973. doi:10.1681/ASN.2015060621
28. Matsuura R, Hiraishi A, Holzman LB, et al. SHROOM3, the gene associated with chronic kidney disease, affects the podocyte structure. *Sci Rep*. 2020;10(1):21103. doi:10.1038/s41598-020-77952-9
29. Holstein-Rathlou NH, Wagner AJ, Marsh DJ. Tubuloglomerular feedback dynamics and renal blood flow autoregulation in rats. *Am J Physiol*. 1991;260(1 Pt 2):F53-68. doi:10.1152/ajprenal.1991.260.1.F53
30. Endlich N, Endlich K. The challenge and response of podocytes to glomerular hypertension. *Semin Nephrol*. 2012;32(4):327-341. doi:10.1016/j.semnephrol.2012.06.004
31. Bode M, Diemer JN, Luu TV, et al. Complement component C3 as a new target to lower albuminuria in hypertensive kidney disease. *Br J Pharmacol*. 2023;180(18):2412-2435. doi:10.1111/bph.16097
32. Dreher L, Bode M, Ehnert N, et al. Role of the anaphylatoxin receptor C5aR2 in angiotensin II induced hypertension and hypertensive end organ damage. *Am J Hypertens*. 2024. doi:10.1093/ajh/hpae082
33. Pfaffl MW. A new mathematical model for relative quantification in real-time RT-PCR. *Nucleic Acids Res*. 2001;29(9):e45. doi:10.1093/nar/29.9.e45
34. Blankenburg S, Hentschker C, Nagel A, et al. Improving Proteome Coverage for Small Sample Amounts: An Advanced Method for Proteomics Approaches with Low Bacterial Cell Numbers. *Proteomics*. 2019;19(23):e1900192. doi:10.1002/pmic.201900192
35. Suomi T, Elo LL. Enhanced differential expression statistics for data-independent acquisition proteomics. *Sci Rep*. 2017;7(1):5869. doi:10.1038/s41598-017-05949-y
36. Dobin A, Davis CA, Schlesinger F, et al. STAR: ultrafast universal RNA-seq aligner. *Bioinformatics*. 2013;29(1):15-21. doi:10.1093/bioinformatics/bts635
37. Liao Y, Smyth GK, Shi W. featureCounts: an efficient general purpose program for assigning sequence reads to genomic features. *Bioinformatics*. 2014;30(7):923-930. doi:10.1093/bioinformatics/btt656
38. Love MI, Huber W, Anders S. Moderated estimation of fold change and dispersion for RNA-seq data with DESeq2. *Genome Biol*. 2014;15(12):550. doi:10.1186/s13059-014-0550-8
39. Patro R, Duggal G, Love MI, Irizarry RA, Kingsford C. Salmon provides fast and bias-aware quantification of transcript expression. *Nat Methods*. 2017;14(4):417-419. doi:10.1038/nmeth.4197
40. Vitting-Seerup K, Sandelin A. IsoformSwitchAnalyzeR: analysis of changes in genome-wide patterns of alternative splicing and its functional consequences. *Bioinformatics*. 2019;35(21):4469-4471. doi:10.1093/bioinformatics/btz247

41. Vaquero-Garcia J, Barrera A, Gazzara MR, et al. A new view of transcriptome complexity and regulation through the lens of local splicing variations. *Elife*. 2016;5:e11752. doi:10.7554/eLife.11752
42. Li YI, Knowles DA, Humphrey J, et al. Annotation-free quantification of RNA splicing using LeafCutter. *Nat Genet*. 2018;50(1):151-158. doi:10.1038/s41588-017-0004-9
43. Sterne-Weiler T, Weatheritt RJ, Best AJ, Ha KCH, Blencowe BJ. Efficient and Accurate Quantitative Profiling of Alternative Splicing Patterns of Any Complexity on a Laptop. *Mol Cell*. 2018;72(1):187-200.e6. doi:10.1016/j.molcel.2018.08.018
44. Wu T, Hu E, Xu S, et al. clusterProfiler 4.0: A universal enrichment tool for interpreting omics data. *Innovation (Camb)*. 2021;2(3):100141. doi:10.1016/j.xinn.2021.100141
45. Kliewe F, Kaling S, Lötzsch H, et al. Fibronectin is up-regulated in podocytes by mechanical stress. *FASEB J*. 2019;33(12):14450-14460. doi:10.1096/fj.201900978RR
46. Gress A, Srikakulam SK, Keller S, Ramensky V, Kalinina OV. d-StructMAn: Containerized structural annotation on the scale from genetic variants to whole proteomes. *Gigascience*. 2022;11. doi:10.1093/gigascience/giac086
47. Püspöki Z, Storath M, Sage D, Unser M. Transforms and Operators for Directional Bioimage Analysis: A Survey. *Adv Anat Embryol Cell Biol*. 2016;219:69-93. doi:10.1007/978-3-319-28549-8_3
48. Friedrich C, Endlich N, Kriz W, Endlich K. Podocytes are sensitive to fluid shear stress in vitro. *Am J Physiol Renal Physiol*. 2006;291(4):F856-65. doi:10.1152/ajprenal.00196.2005
49. Gilbert W. Why genes in pieces? *Nature*. 1978;271(5645):501. doi:10.1038/271501a0
50. McManus CJ, Graveley BR. RNA structure and the mechanisms of alternative splicing. *Curr Opin Genet Dev*. 2011;21(4):373-379. doi:10.1016/j.gde.2011.04.001
51. Ostalska-Nowicka D, Zachwieja J, Nowicki M, Kaczmarek E, Siwinska A, Witt M. Ezrin--a useful factor in the prognosis of nephrotic syndrome in children: an immunohistochemical approach. *J Clin Pathol*. 2006;59(9):916-920. doi:10.1136/jcp.2005.031732
52. Wasik AA, Koskelainen S, Hyvönen ME, et al. Ezrin is down-regulated in diabetic kidney glomeruli and regulates actin reorganization and glucose uptake via GLUT1 in cultured podocytes. *Am J Pathol*. 2014;184(6):1727-1739. doi:10.1016/j.ajpath.2014.03.002
53. Kobayashi N, Ueno T, Ohashi K, et al. Podocyte injury-driven intracapillary plasminogen activator inhibitor type 1 accelerates podocyte loss via uPAR-mediated β1-integrin endocytosis. *Am J Physiol Renal Physiol*. 2015;308(6):F614-26. doi:10.1152/ajprenal.00616.2014
54. Ogino S, Yoshikawa K, Nagase T, Mikami K, Nagase M. Roles of the mechanosensitive ion channel Piezo1 in the renal podocyte injury of experimental hypertensive nephropathy. *Hypertens Res*. 2024;47(3):747-759. doi:10.1038/s41440-023-01536-z
55. Reiser J, Polu KR, Möller CC, et al. TRPC6 is a glomerular slit diaphragm-associated channel required for normal renal function. *Nat Genet*. 2005;37(7):739-744. doi:10.1038/ng1592
56. Faul C, Asanuma K, Yanagida-Asanuma E, Kim K, Mundel P. Actin up: regulation of podocyte structure and function by components of the actin cytoskeleton. *Trends Cell Biol*. 2007;17(9):428-437. doi:10.1016/j.tcb.2007.06.006
57. Endlich K, Kliewe F, Endlich N. Stressed podocytes-mechanical forces, sensors, signaling and response. *Pflugers Arch*. 2017;469(7-8):937-949. doi:10.1007/s00424-017-2025-8
58. Rauen T, Frye BC, Wang J, et al. Cold shock protein YB-1 is involved in hypoxia-dependent gene transcription. *Biochem Biophys Res Commun*. 2016;478(2):982-987. doi:10.1016/j.bbrc.2016.08.064
59. Lindquist JA, Mertens PR. Cold shock proteins: from cellular mechanisms to pathophysiology and disease. *Cell Commun Signal*. 2018;16(1):63. doi:10.1186/s12964-018-0274-6
60. Luimula P, Aaltonen P, Ahola H, Palmen T, Holthöfer H. Alternatively spliced nephrin in experimental glomerular disease of the rat. *Pediatr Res*. 2000;48(6):759-762. doi:10.1203/00006450-200012000-00010

61. Wagner N, Wagner K-D, Xing Y, Scholz H, Schedl A. The major podocyte protein nephrin is transcriptionally activated by the Wilms' tumor suppressor WT1. *J Am Soc Nephrol*. 2004;15(12):3044-3051. doi:10.1097/01.ASN.0000146687.99058.25
62. Haber DA, Sohn RL, Buckler AJ, Pelletier J, Call KM, Housman DE. Alternative splicing and genomic structure of the Wilms tumor gene WT1. *Proc Natl Acad Sci U S A*. 1991;88(21):9618-9622. doi:10.1073/pnas.88.21.9618
63. Broghammer H, Bernhart W. Friedrich Carl Bessel-Hagen, Chirurg und Anthropologe (2.1.1856-20.12.1945). *Zentralbl Chir*. 1997;122(12):1152-1157.
64. Lefebvre J, Clarkson M, Massa F, et al. Alternatively spliced isoforms of WT1 control podocyte-specific gene expression. *Kidney Int*. 2015;88(2):321-331. doi:10.1038/ki.2015.140
65. Sugnet CW, Kent WJ, Ares M, Haussler D. Transcriptome and genome conservation of alternative splicing events in humans and mice. *Pac Symp Biocomput*. 2004:66-77. doi:10.1142/9789812704856_0007
66. Shen S, Park JW, Lu Z, et al. rMATS: robust and flexible detection of differential alternative splicing from replicate RNA-Seq data. *Proc Natl Acad Sci U S A*. 2014;111(51):E5593-601. doi:10.1073/pnas.1419161111
67. Olivieri JE, Dehghannasiri R, Wang PL, et al. RNA splicing programs define tissue compartments and cell types at single-cell resolution. *Elife*. 2021;10. doi:10.7554/eLife.70692
68. Lee C, Le M-P, Wallingford JB. The shroom family proteins play broad roles in the morphogenesis of thickened epithelial sheets. *Dev Dyn*. 2009;238(6):1480-1491. doi:10.1002/dvdy.21942
69. Park I, Han C, Jin S, et al. Myosin regulatory light chains are required to maintain the stability of myosin II and cellular integrity. *Biochem J*. 2011;434(1):171-180. doi:10.1042/BJ20101473
70. Brito C, Sousa S. Non-Muscle Myosin 2A (NM2A): Structure, Regulation and Function. *Cells*. 2020;9(7). doi:10.3390/cells9071590
71. Paul A, Lawlor A, Cunanan K, et al. The Good and the Bad of SHROOM3 in Kidney Development and Disease: A Narrative Review. *Can J Kidney Health Dis*. 2023;10:20543581231212038. doi:10.1177/20543581231212038
72. Riento K, Ridley AJ. Rocks: multifunctional kinases in cell behaviour. *Nat Rev Mol Cell Biol*. 2003;4(6):446-456. doi:10.1038/nrm1128
73. Nishimura T, Takeichi M. Shroom3-mediated recruitment of Rho kinases to the apical cell junctions regulates epithelial and neuroepithelial planar remodeling. *Development*. 2008;135(8):1493-1502. doi:10.1242/dev.019646
74. Plageman TF, Chauhan BK, Yang C, et al. A Trio-RhoA-Shroom3 pathway is required for apical constriction and epithelial invagination. *Development*. 2011;138(23):5177-5188. doi:10.1242/dev.067868
75. Amano M, Ito M, Kimura K, et al. Phosphorylation and activation of myosin by Rho-associated kinase (Rho-kinase). *J Biol Chem*. 1996;271(34):20246-20249. doi:10.1074/jbc.271.34.20246
76. Kimura K, Ito M, Amano M, et al. Regulation of myosin phosphatase by Rho and Rho-associated kinase (Rho-kinase). *Science*. 1996;273(5272):245-248. doi:10.1126/science.273.5272.245
77. Matsumura F. Regulation of myosin II during cytokinesis in higher eukaryotes. *Trends Cell Biol*. 2005;15(7):371-377. doi:10.1016/j.tcb.2005.05.004
78. Mohan S, Rizaldy R, Das D, et al. Structure of Shroom domain 2 reveals a three-segmented coiled-coil required for dimerization, Rock binding, and apical constriction. *Mol Biol Cell*. 2012;23(11):2131-2142. doi:10.1091/mbc.E11-11-0937
79. Perez-Moreno M, Jamora C, Fuchs E. Sticky business: orchestrating cellular signals at adherens junctions. *Cell*. 2003;112(4):535-548. doi:10.1016/s0092-8674(03)00108-9

80. Vogelmann R, Nelson WJ. Fractionation of the epithelial apical junctional complex: reassessment of protein distributions in different substructures. *Mol Biol Cell*. 2005;16(2):701-716. doi:10.1091/mbc.e04-09-0827
81. Ransick A, Lindström NO, Liu J, et al. Single-Cell Profiling Reveals Sex, Lineage, and Regional Diversity in the Mouse Kidney. *Dev Cell*. 2019;51(3):399-413.e7. doi:10.1016/j.devcel.2019.10.005
82. Chung J-J, Goldstein L, Chen Y-JJ, et al. Single-Cell Transcriptome Profiling of the Kidney Glomerulus Identifies Key Cell Types and Reactions to Injury. *J Am Soc Nephrol*. 2020;31(10):2341-2354. doi:10.1681/ASN.2020020220
83. Rinschen MM, Gödel M, Grahammer F, et al. A Multi-layered Quantitative In Vivo Expression Atlas of the Podocyte Unravels Kidney Disease Candidate Genes. *Cell Rep*. 2018;23(8):2495-2508. doi:10.1016/j.celrep.2018.04.059
84. Nakagawa S, Nishihara K, Miyata H, et al. Molecular Markers of Tubulointerstitial Fibrosis and Tubular Cell Damage in Patients with Chronic Kidney Disease. *PLoS One*. 2015;10(8):e0136994. doi:10.1371/journal.pone.0136994

Acknowledgements

The authors thank Anja Wiechert, Claudia Weber, and Sophia-Marie Bach for technical assistance.

This work was supported by grants of the Federal Ministry of Education and Research (BMBF, grant 01ZX1908B + 01ZX2208B, Sys_CARE) to Jan Baumbach, Uwe Völker, and Nicole Endlich. This work was generously supported by the Südmeyer fund for kidney and vascular research (‘Südmeyer Stiftung für Nieren- und Gefäßforschung') and the Dr. Gerhard Büchtemann fund, Hamburg, Germany. The funders had no role in study design, data collection and analysis, decision to publish, or preparation of the manuscript.

Figure Legends

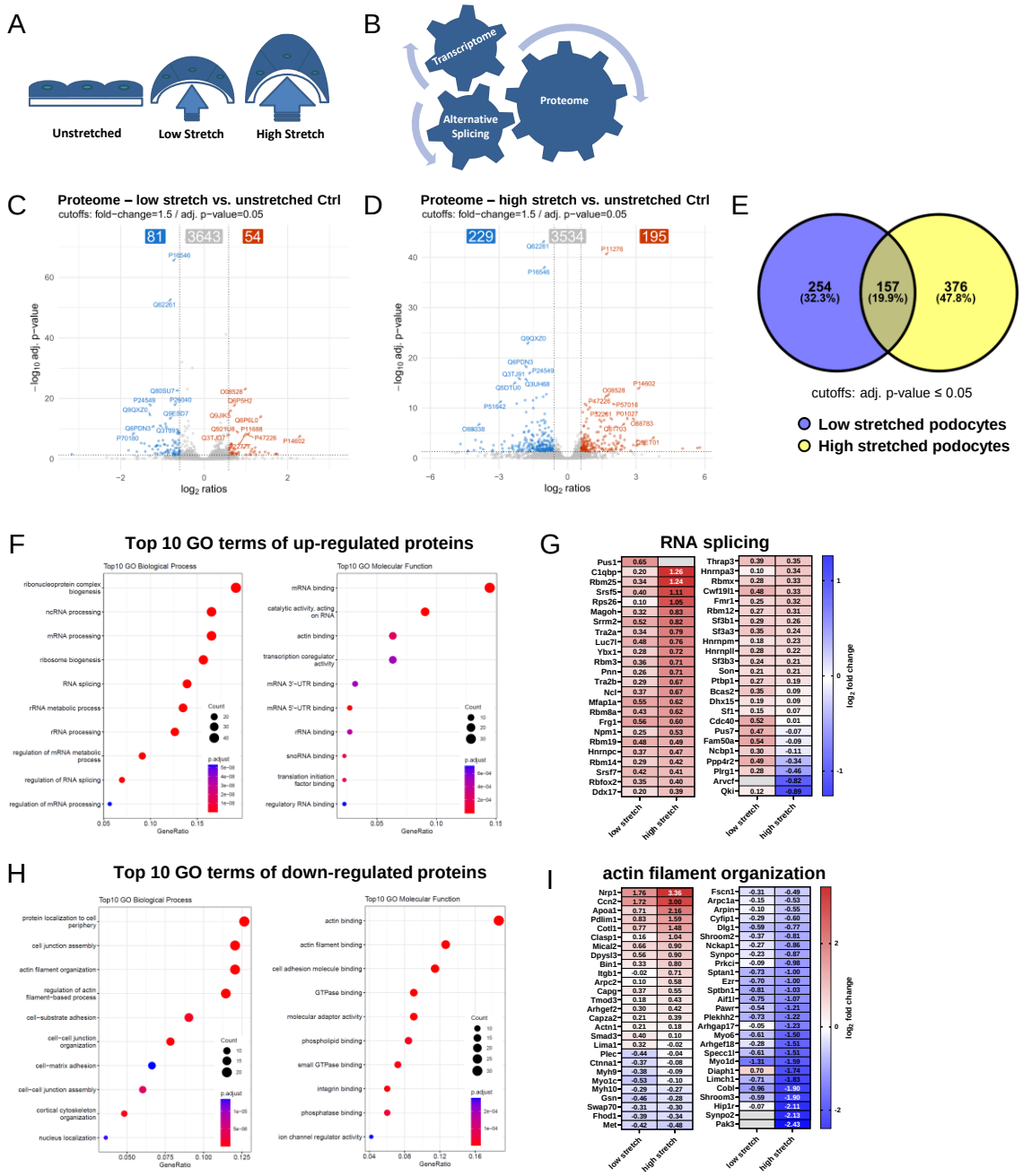

Fig. 1: Proteomics of mechanically stretched podocytes.
(A) Schematic representation of the different stretch conditions. (B) RNA and proteins from the stretched podocytes were analyzed by RNA-Seq and LC-MS/MS to investigate the mutual influence of the transcriptome and alternative splicing on the proteome. (C, D) Volcano plot displaying the significantly changed proteins upon (C) low and (D) high stretch conditions. Given are proteins with a fold-change ≥ 1.5 and adjusted p-value ≤ 0.05. (E) Venn diagram depicts overlap of 157 proteins that are significantly regulated at low and high stretch conditions (cutoffs: adj. p-value ≤ 0.05). (F) Top 10 GO (Gene Ontology) clusters in podocytes, based on significantly up-regulated proteins in mechanically stretched podocytes compared to unstretched Ctrl. (G) Heatmap (LC-MS/MS based relative protein level) of regulated "RNA splicing" proteins (GO term) in low and high stretched podocytes. Data are represented as log2 fold change, a p-value < 0.05 was considered as significant. Red: up-regulated; blue: down-regulated compared to controls. (H) Top 10 GO (Gene Ontology) clusters in podocytes, based on significantly down-regulated proteins in mechanically stretched podocytes compared to unstretched Ctrl. (I) Heatmap (LC-MS/MS based relative protein level) of regulated "actin filament organization" proteins (GO term) in low and high stretched podocytes. Data are presented as in Fig. G.

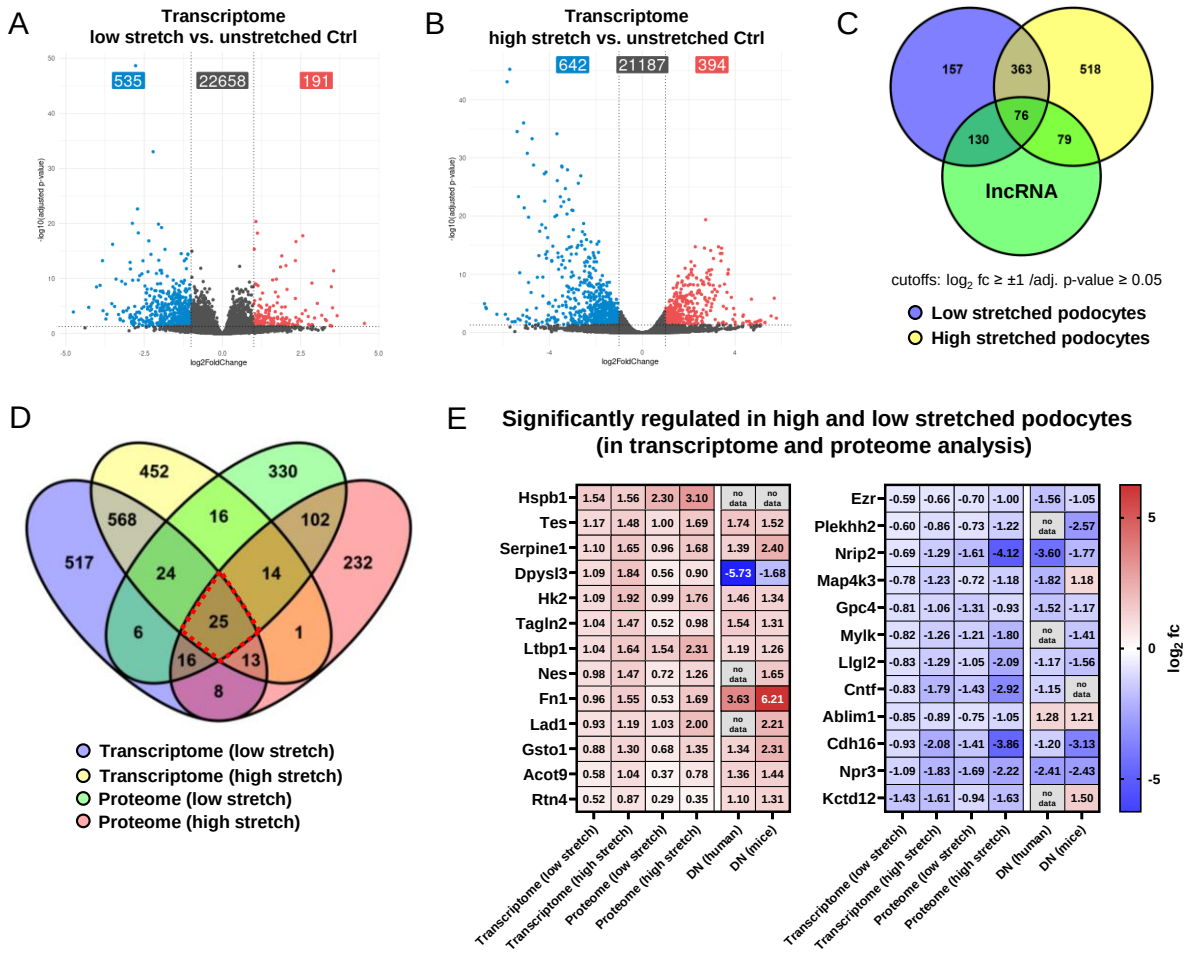

Fig. 2: RNA-Seq data of mechanically stretched podocytes.
(A, B) Volcano plot displaying the significantly changed genes at (A) low and (B) high stretch conditions. Given are genes with a log2 fold-change ≥ 1 and adjusted p-value ≤ 0.05. (C) Venn diagram shows overlap of 76 proteins that are significantly regulated at low and high stretch conditions and belong to the lncRNAs (cutoffs: adj. p-value ≤ 0.05 and log2 fold change ≥ 1). (D) Venn diagram depicts overlap of 25 proteins that are significantly regulated at low and high stretch conditions in the transcriptome analysis (cutoffs: adj. p-value ≤ 0.05 and log2 fold change ≥ 0.5) as well as in the proteome (cutoffs: adj. p-value ≤ 0.05). (E) Heatmap of significantly regulated genes/proteins in low and high stretched podocytes. In addition, the expression of the candidates in DN patients or DN mice is shown (data from Nephroseq). Data are represented as log2 fold change, a p-value < 0.05 was considered as significant. Red: up-regulated; blue: down-regulated compared to controls.

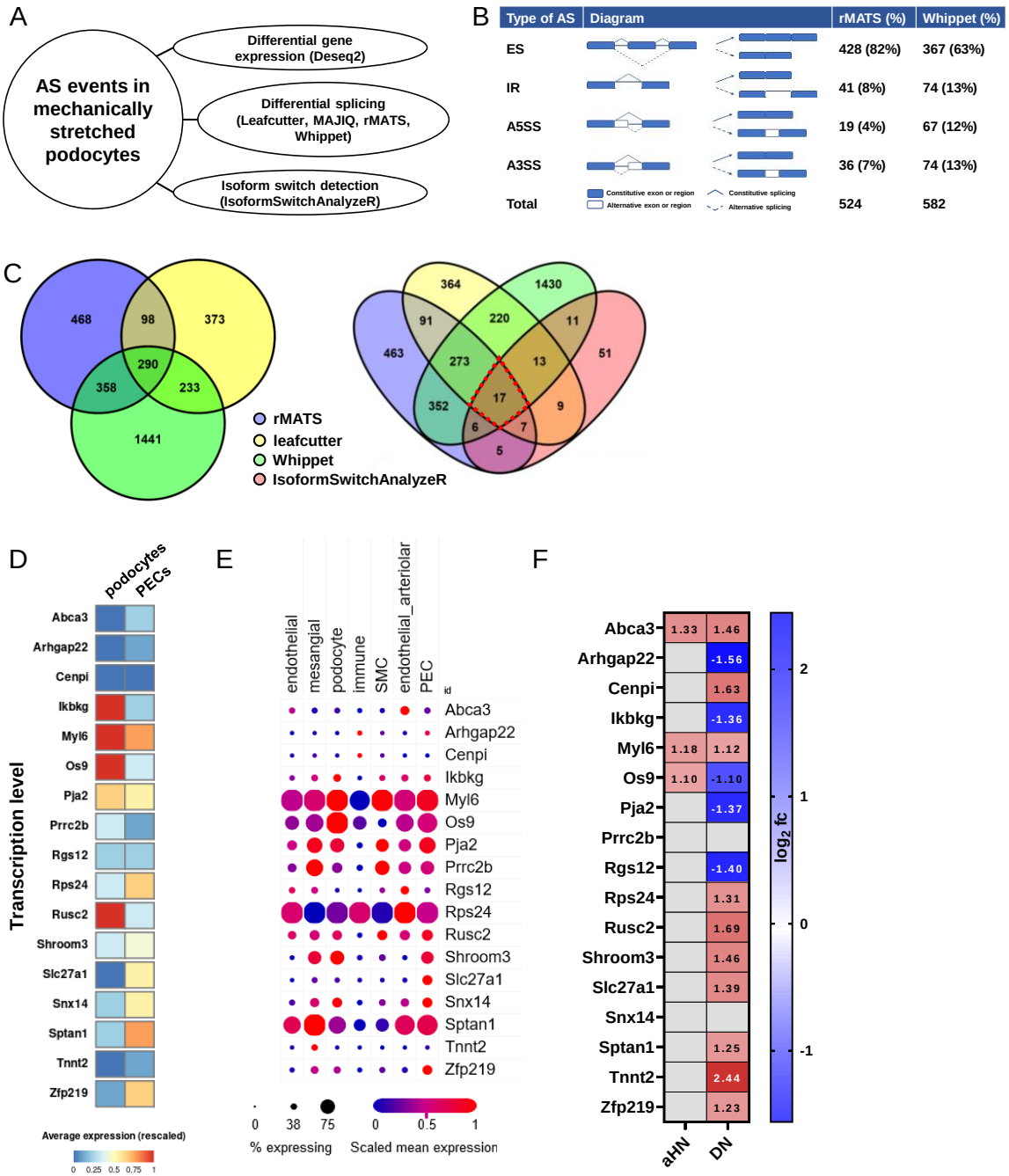

Fig. 3: Alternative spliced transcripts in mechanically stretched podocytes.
(A) Procedure of the AS event analysis. (B) Overview of the found AS types: ES (exon skipping); IR (intron retention); A5SS (Alternative 5′ splice site); A3SS (Alternative 3′ splice site). Only those AS events were considered which were significantly and have a deltaPSI > 0.1 (C) Venn diagram depicts overlap of 290 genes that showed a significant splice event in rMATS, leafcutter and Whippet. When filtering more stringently for the transcripts that also show an isoform switch (by using IsoformSwitchAnalyzer), 17 candidates remain. (D) Database analysis using the Kidney Cell Explorer by Ransick et al.[81] based on a single-cell RNA sequencing data set of murine kidneys to determine podocyte-specific expression. Figure S6 shows expression pattern from all kidney cell fractions. Color code: Red means a high average expression; Blue: low expression. (E) Single-cell RNA-Seq data of mouse glomerulus (published from Chung et al.[82] and available at https://singlecell.broadinstitute.org/single_cell). (F) mRNA expression level of renal glomeruli from mice with arterial hypertension (aHN) or human patients with diabetic nephropathy (DN). Data were taken from Nephroseq Research Edition (Ann Arbor, University of Michigan) and are represented as log2 fold change, a q-value < 0.05 was considered as significant. Red: up-regulated; blue: down-regulated compared to control.

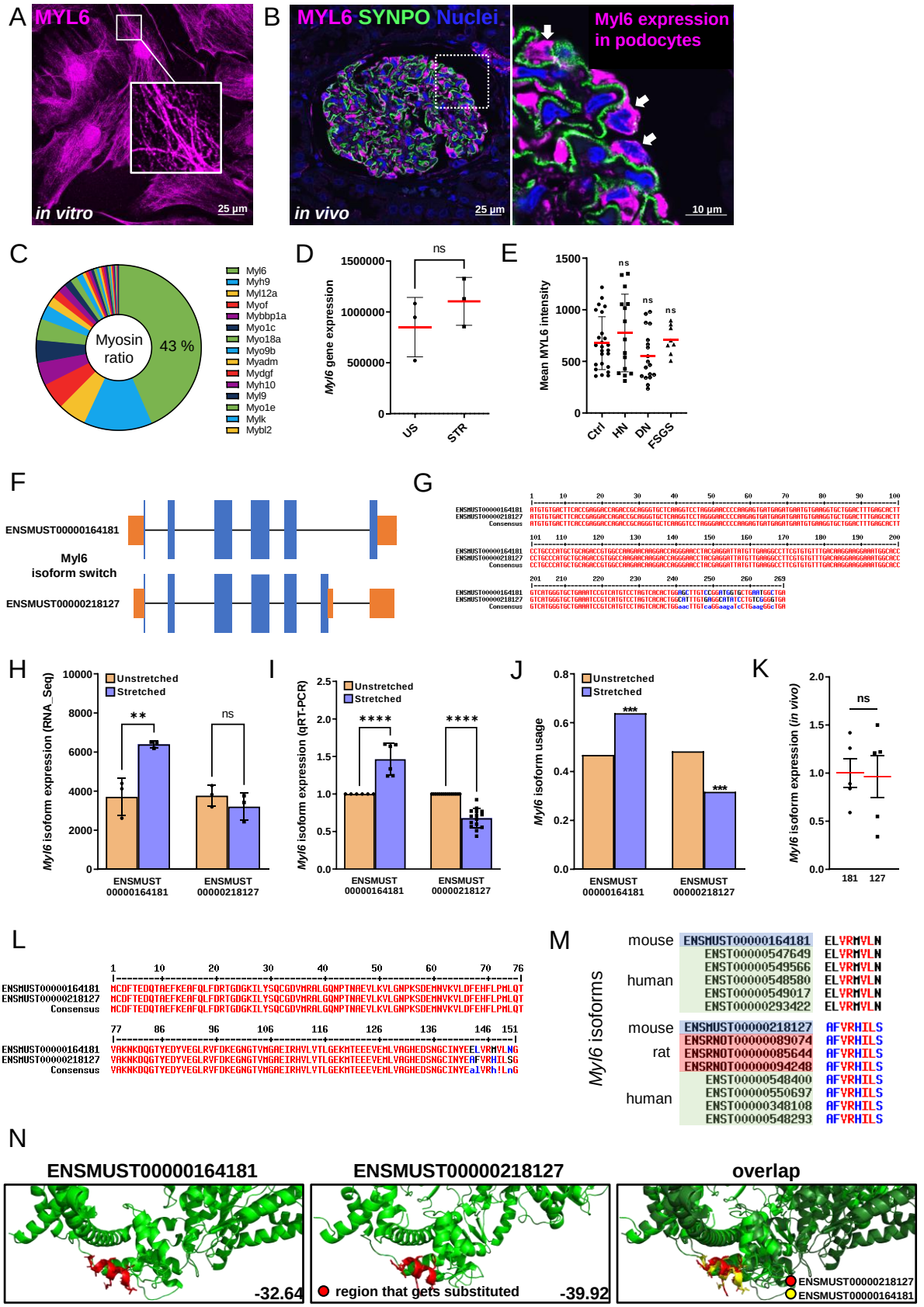

Fig. 4: *Myl6* coded transcripts are alternative spliced in mechanically stretched podocytes. (A) Immunofluorescence staining of MYL6 (magenta) showed high abundance in murine cultured podocytes. Scale bar represents 25 µm. (B) MYL6 (shown in magenta) is also expressed *in vivo* from podocytes (marked by white arrow heads). Synaptopodin is shown in green. Nuclei were stained with Hoechst (blue). Scale bars represent 25 µm and 10 µm (magnification) respectively. (C) Overview of the expression distribution of all myosin proteins found in podocytes. (D) *Myl6* gene expression in

unstretched (US) und stretched (STR) podocytes. (E) Mean MYL6 fluorescence intensity in Ctrl, HN, DN and FSGS patients. Each dot represents the mean from one individual glomerulus (n≥15). (F) Schematic overview of the two Myl6 isoforms found in murine cultured podocytes. Blue: coding exons; Orange: untranslated regions. (G) Sequence alignment of coding exons of both *Myl6* isoforms. (H) *Myl6* isoform expression based on RNA-Seq data. (I) Validation of *Myl6* isoform expression by qRT-PCR. (J) *Myl6* isoform usage based on IsoformSwitchAnalyzer data. (K) *In vivo Myl6* transcript expression in isolated mouse glomeruli determined by qRT-PCR. (L) Protein sequence alignment of both MYL6 isoforms. (M) Amino acid switch from ELVRMVLN to AFVRHILS is well conserved in mouse, rat, and human. (N) Protein structural analyses revealed that amino acid substitution weakens the actin interaction surface. Data are presented as means ± SD. ** $p<0.01$; *** $p<0.001$; **** $p<0.0001$; ns, not significant.

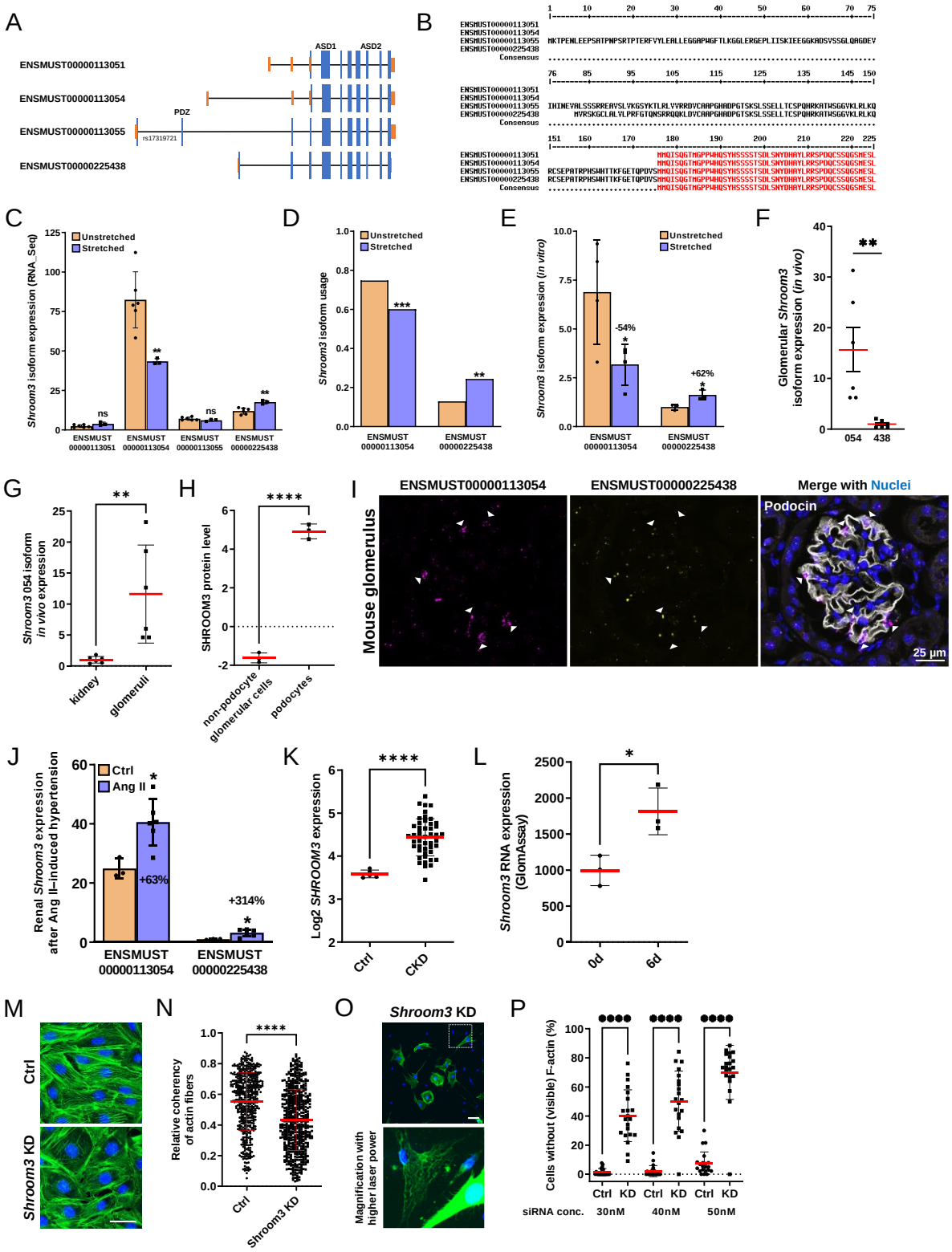

Fig. 5: Alternative spliced isoforms of *Shroom3* in mechanically stretched podocytes.
(A) Schematic overview of all *Shroom3* isoforms found in murine cultured podocytes. PDZ domain and ABD (actin binding domain) are marked. Blue: coding exons; Orange: untranslated regions (UTRs). (B) Protein sequence alignment of all SHROOM3 isoforms. Shown are the first 225 amino acids; complete sequence is shown in Fig. S7. (C) *Shroom3* isoform expression based on RNA-Seq data. (D) *Shroom3* coded isoform usage based on IsoformSwitchAnalyzer data. (E) Validation of *Shroom3* isoform switch by qRT-PCR. (F) qRT-PCR confirmed that transcript ENSMUST00000113054 is significantly higher expressed in *in vivo* glomeruli than ENSMUST00000225438. (G) *Shroom3* isoform 054 expression in whole kidney and isolated glomeruli. qRT-PCR experiments were normalized to the kidney samples and

Gapdh. (H) Podocyte proteome data showed an enrichment of SHROOM3 protein level in podocytes compared to non-podocyte glomerular cells. Data from Rinschen et al.[83]. (I) Both isoforms of *Shroom3* were detected at different levels by *in situ* hybridization. Immunostaining of podocin is shown in white. Nuclei stained with Hoechst (blue). Scale bar represents 25 µm. (J) mRNA expression of *Shroom3* in murine kidneys with angiotensin II-induced hypertension (n=6) compared to Ctrl (n=3). (K) Analysis of human glomerular disease data[84] (Nephroseq database) further substantiated increased expression on mRNA levels of *SHROOM3* in CKD patients (n = 47) compared to healthy controls (Ctrl) (n = 5). (L) *Shroom3* mRNA level of isolated glomeruli until 6 days of cultivation and transdifferentiation. The mRNA fold enrichment was normalized to day 0 and showed a significant increase of *Shroom3* expression. (M) Immunofluorescence staining of F-actin (green) of *Shroom3* KD and control (Ctrl) podocytes (transfected with non targeting control siRNA). Knockdown of *Shroom3* leads to a formation of an unorganized actin cytoskeleton. Nuclei were stained with DAPI (blue). Scale bar represents 100 µm. (N) The relative coherency of actin fibers was measured using OrientationJ (n = 3; each 20 analyzed cells; means ± SD). (O) *Shroom3* KD leads to dramatic reduction in F-actin formation. F-Actin is shown in green. Nuclei were stained with DAPI (blue). Scale bar represents 100 µm. (P) Percentage of cells without (visible) F-actin compared to controls (transfected with negative scrambled siRNA). * $p<0.05$; ** $p<0.01$; *** $p<0.001$; **** $p<0.0001$;ns, not significant.

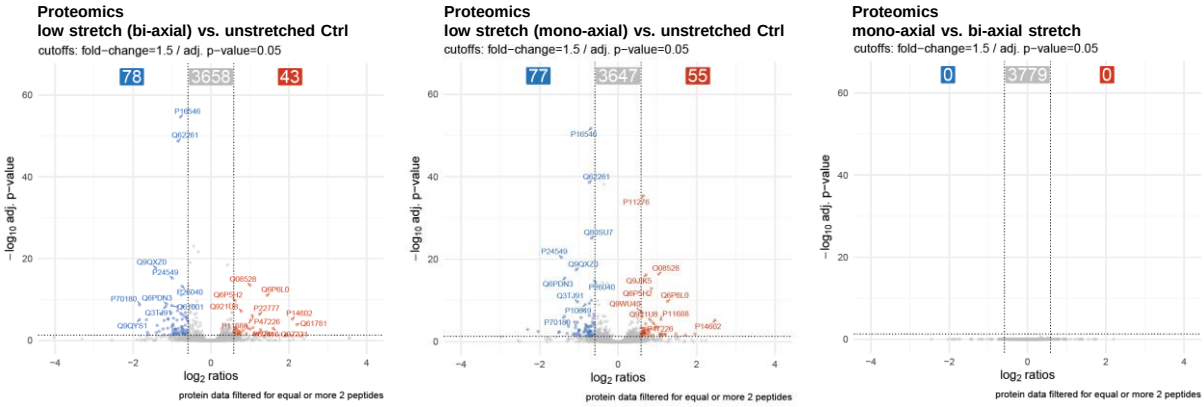

Fig. S1: Mono-axial and bi-axial movement of the membrane expansion result in a similar expression pattern.

Volcano plot of the significantly changed proteins with bi-axial and mono-axial stretch apparatuses compared to unstretched podocytes. Direct comparison did not reveal significantly differentially regulated proteins between the different stretch apparatuses. Given are proteins with a fold-change ≥ 1.5 and adjusted p-value ≤ 0.05.

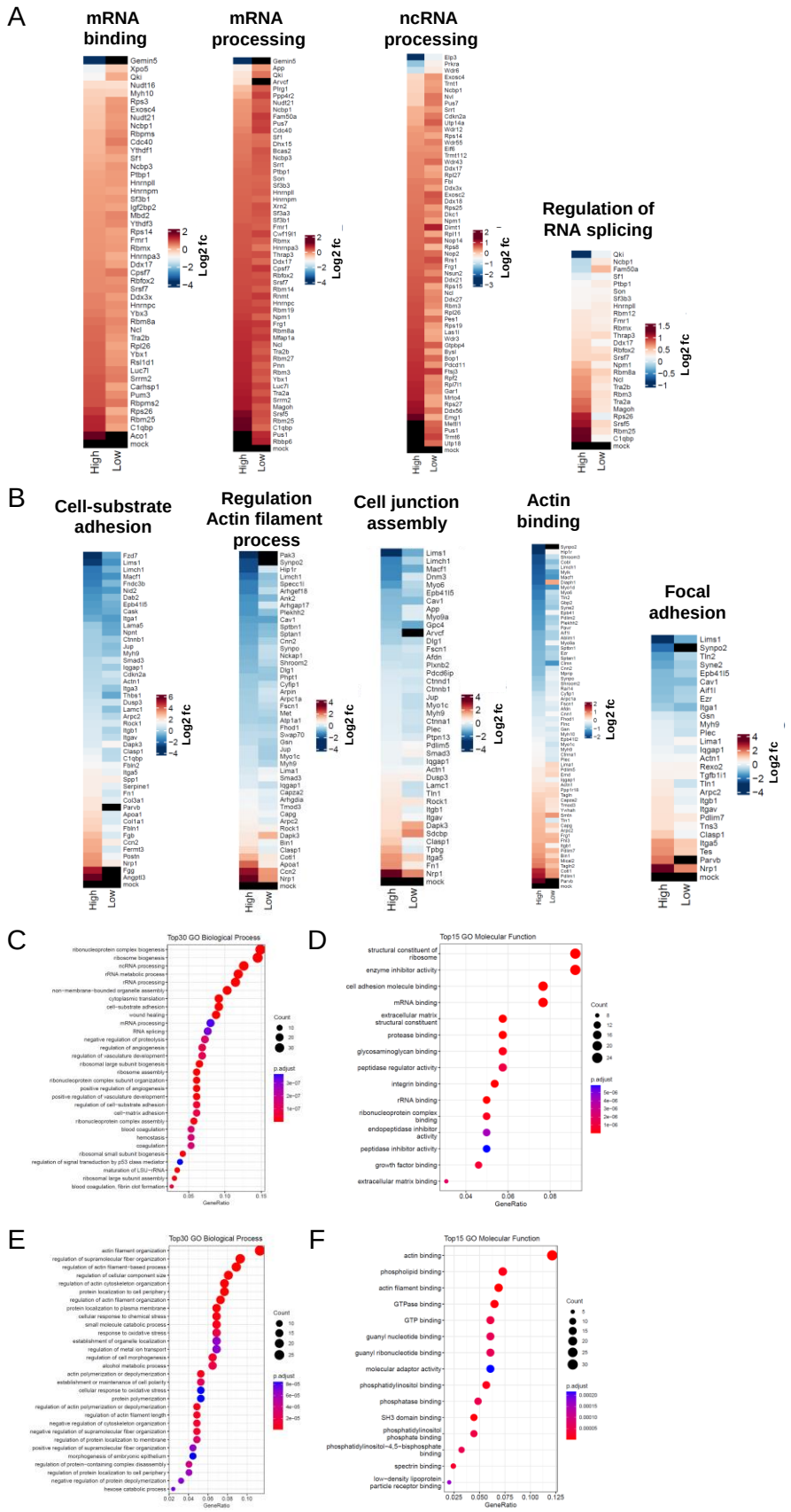

Fig. S2: GO and GSEA from mechanically stretched podocytes (proteome based).
Heatmap of GO terms of (A) up-regulated and (B) down-regulated proteins in high stretched podocytes. Data are represented as log2 fold change, a p-value < 0.05 was considered as significant. Red: up-regulated; blue: down-regulated compared to controls. (C-F) GO (Gene Ontology) clusters (Biological Process and Molecular Function) of low stretched podocytes.

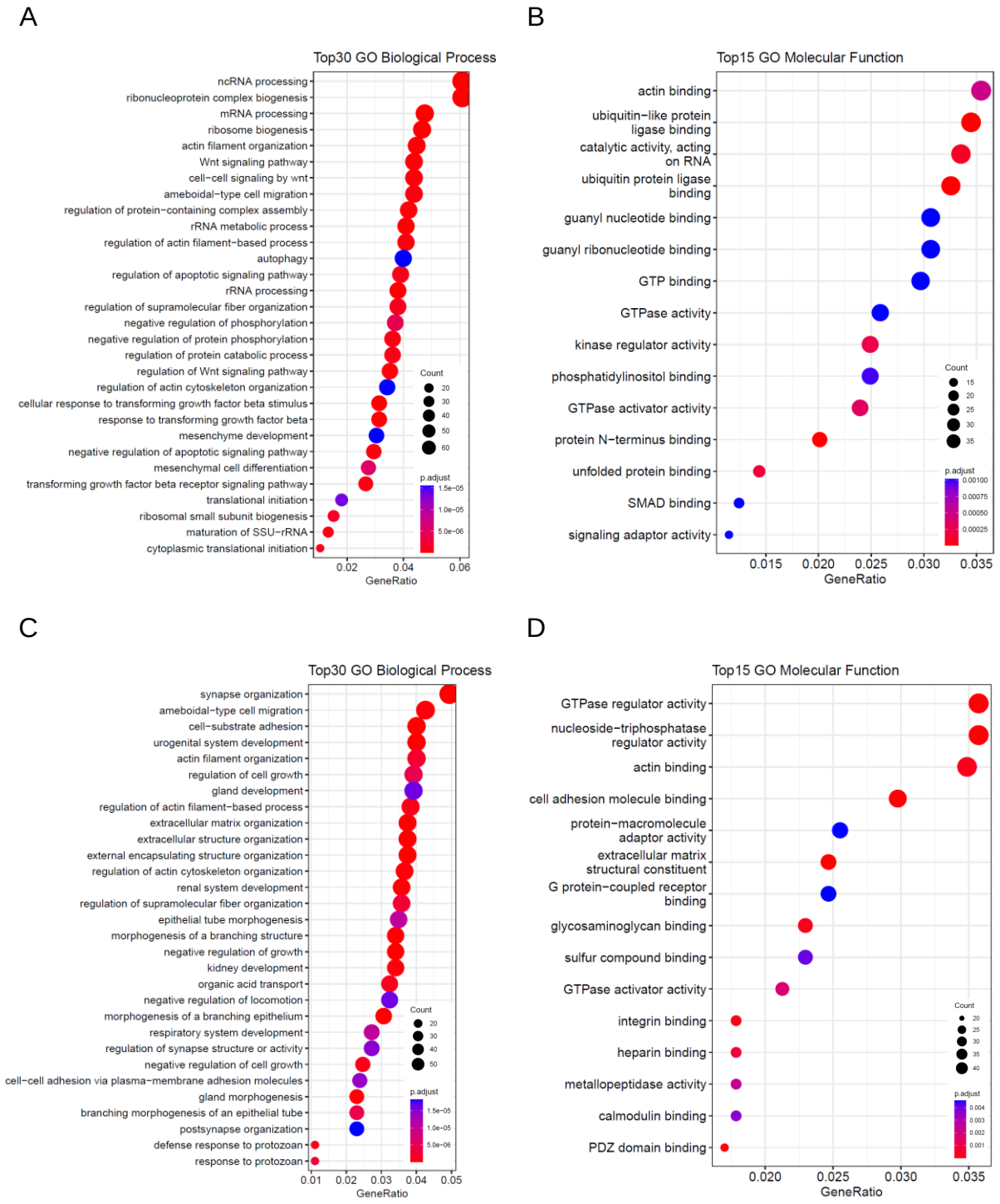

Fig. S3: Detailed gene set enrichment analysis (GSEA) of significantly regulated genes (transcriptome based).

(A-D) RNA-Seq based enriched Top30 GO (Gene Ontology) clusters (Biological Process and Molecular Function) of mechanically stretched podocytes. Demonstrated are GO clusters from differentially up-regulated transcripts (A; B) and down-regulated transcripts (C; D).

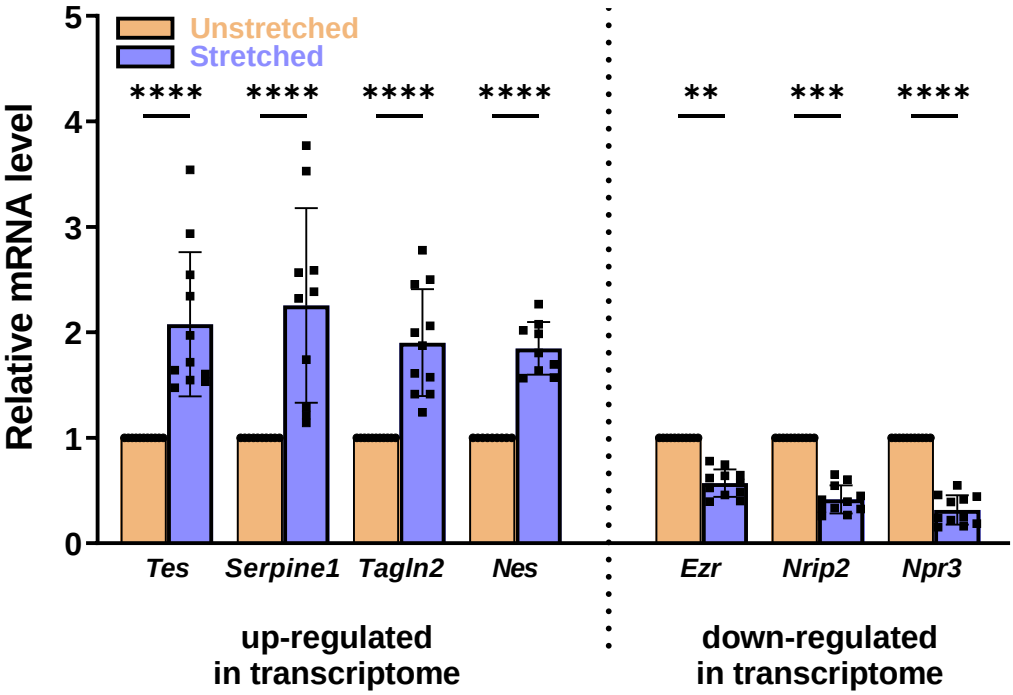

Fig. S4: Verification of up- and down-regulated candidates from Fig. 2.
(A) The mRNA expression of *Tes*, *Serpine11*, *Tagln2*, *Nes*, *Ezr*, *Nrip2,* and *Npr3* in stretched and unstretched podocytes was quantified by qRT-PCR (n≥9). qRT-PCR experiments were normalized to the unstretched samples, *Gapdh* served as a reference. Data are presented as means ± SD. ** $p<0.01$; *** $p<0.001$; **** $p<0.0001$.

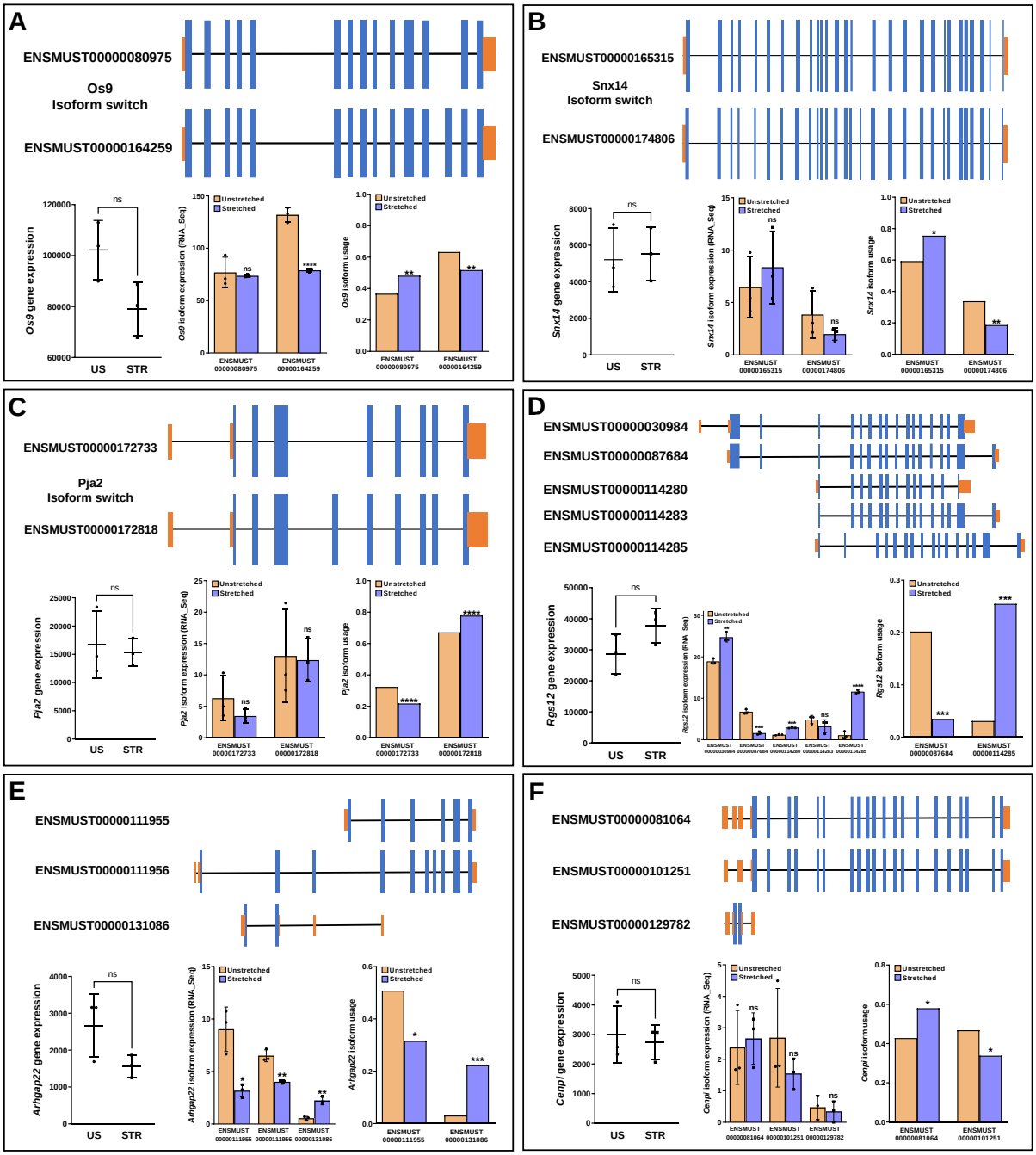

Fig. S5: Isoform switch detection of Os9, Snx14, Pja2, Rgs12, Arhgap22 and Cenpi.
Schematic overview of A) *Os9*, B) *Snx14*, C) *Pja2*, D) *Rgs12*, E) *Arhgap22* and F) *Cenpi* isoforms found in murine cultured podocytes (Blue: coding exons; Orange: untranslated regions). Each partial figure displays the corresponding gene and transcript expression in unstretched (US) and mechanically stretched (STR) podocytes, as well as isoform usage based on IsoformSwitchAnalyzer data. Data are presented as means ± SD. * $p<0.05$; ** $p<0.01$; *** $p<0.001$; **** $p<0.0001$; ns, not significant.

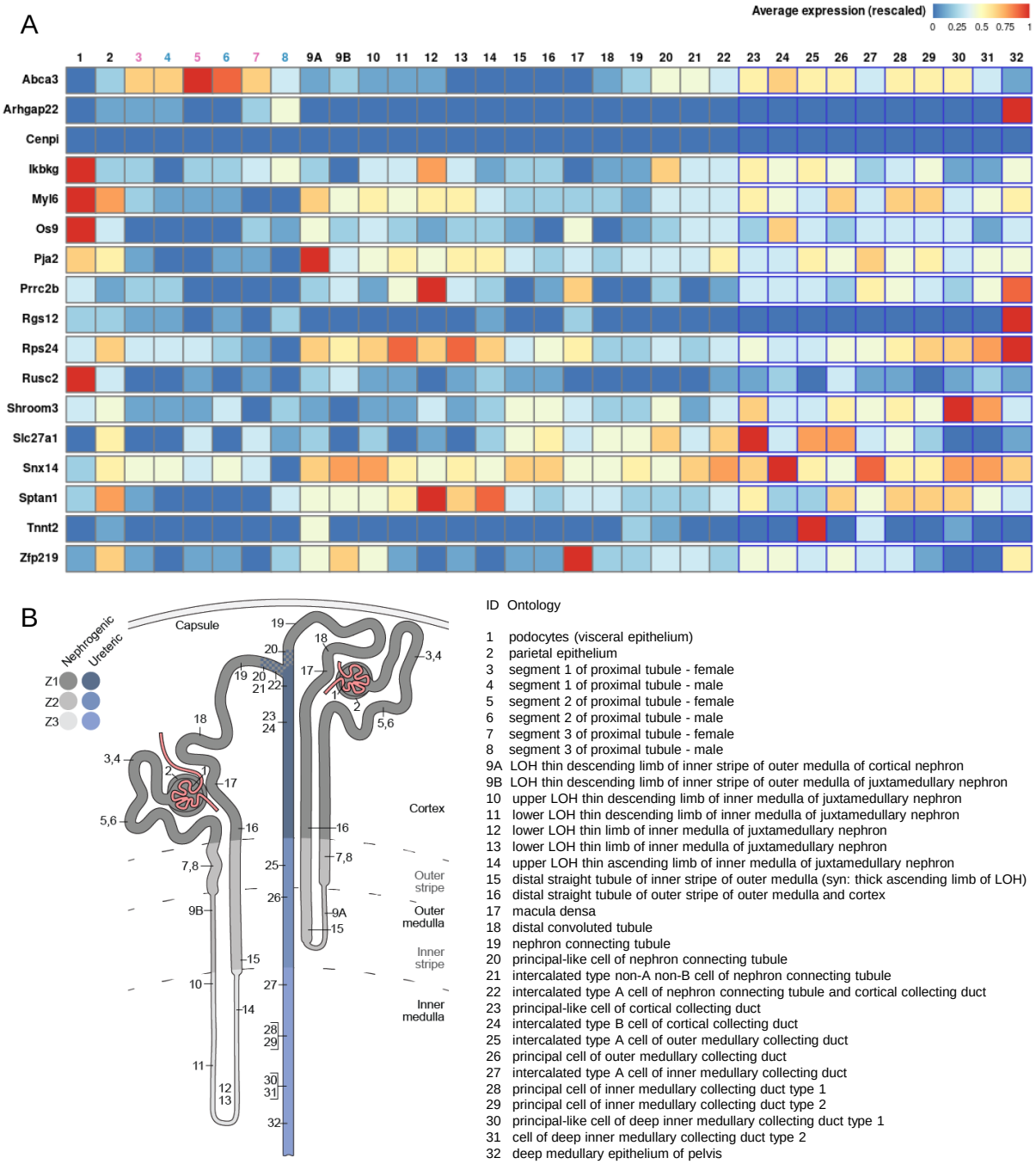

Fig. S6: Kidney expression pattern of RNA-Seq based alternative spliced candidates.
(A) Database analysis using the Kidney Cell Explorer by Ransick et al.[81] based on a single-cell RNA sequencing data set of murine kidneys showed the expression pattern for all kidney cell fractions. Color code: Red means a high average expression; Blue: low expression. (B) Legend of the numerical labeling of figure A.

```
                 1       10        20        30        40        50        60        70        80        90       100       110       120       130
                 |--------+---------+---------+---------+---------+---------+---------+---------+---------+---------+---------+---------+---------|
ENSMUST00000113051
ENSMUST00000113054
ENSMUST00000113055 MKTPENLEEPSATPNPSRTPTERFVYLEALLEGGAPWGFTLKGGLERGEPLIISKIEEGGKADSVSSGLQAGDEVIHINEVALSSSRREAVSLVKGSYKTLRLYVRRDVCAAPGHADPGTSKSLSSELLT
ENSMUST00000225438                                                                                                   MVRSKGCLALVLPRFGTQNSRRQQKLDVCAAPGHADPGTSKSLSSELLT
        Consensus  ..................................................................................................................................

                 131     140       150       160       170       180       190       200       210       220       230       240       250       260
                 |--------+---------+---------+---------+---------+---------+---------+---------+---------+---------+---------+---------+---------|
ENSMUST00000113051                                                  MMQISQGTMGPPWHQSYHSSSSTSDLSNYDHAYLRRSPDQCSSQGSMESLEPSGGYPPCHLLSPAKSTSSIDQLGHLHNKRDSAY
ENSMUST00000113054                                                  MMQISQGTMGPPWHQSYHSSSSTSDLSNYDHAYLRRSPDQCSSQGSMESLEPSGGYPPCHLLSPAKSTSSIDQLGHLHNKRDSAY
ENSMUST00000113055 CSPQHRKATWSGGVKLRLKQRCSEPATRPHSWHTTKFGETQPDVSMMQISQGTMGPPWHQSYHSSSSTSDLSNYDHAYLRRSPDQCSSQGSMESLEPSGGYPPCHLLSPAKSTSSIDQLGHLHNKRDSAY
ENSMUST00000225438 CSPQHRKATWSGGVKLRLKQRCSEPATRPHSWHTTKFGETQPDVSMMQISQGTMGPPWHQSYHSSSSTSDLSNYDHAYLRRSPDQCSSQGSMESLEPSGGYPPCHLLSPAKSTSSIDQLGHLHNKRDSAY
        Consensus  ........................................MMQISQGTMGPPWHQSYHSSSSTSDLSNYDHAYLRRSPDQCSSQGSMESLEPSGGYPPCHLLSPAKSTSSIDQLGHLHNKRDSAY

                 261     270       280       290       300       310       320       330       340       350       360       370       380       390
                 |--------+---------+---------+---------+---------+---------+---------+---------+---------+---------+---------+---------+---------|
ENSMUST00000113051 SSFSTSSSIFEYPPPGGSARERSGSMDVISARGGLLEGMRQADIRYVKTVYDTRRGVSSEYEVNPSALLLQGRDAHASADSQGCAKWHSIPRGKGTPSPSWSQQCSGSLETATDNLPQKAGAPLPPTRSD
ENSMUST00000113054 SSFSTSSSIFEYPPPGGSARERSGSMDVISARGGLLEGMRQADIRYVKTVYDTRRGVSSEYEVNPSALLLQGRDAHASADSQGCAKWHSIPRGKGTPSPSWSQQCSGSLETATDNLPQKAGAPLPPTRSD
ENSMUST00000113055 SSFSTSSSIFEYPPPGGSARERSGSMDVISARGGLLEGMRQADIRYVKTVYDTRRGVSSEYEVNPSALLLQGRDAHASADSQGCAKWHSIPRGKGTPSPSWSQQCSGSLETATDNLPQKAGAPLPPTRSD
ENSMUST00000225438 SSFSTSSSIFEYPPPGGSARERSGSMDVISARGGLLEGMRQADIRYVKTVYDTRRGVSSEYEVNPSALLLQGRDAHASADSQGCAKWHSIPRGKGTPSPSWSQQCSGSLETATDNLPQKAGAPLPPTRSD
        Consensus  SSFSTSSSIFEYPPPGGSARERSGSMDVISARGGLLEGMRQADIRYVKTVYDTRRGVSSEYEVNPSALLLQGRDAHASADSQGCAKWHSIPRGKGTPSPSWSQQCSGSLETATDNLPQKAGAPLPPTRSD

                 391     400       410       420       430       440       450       460       470       480       490       500       510       520
                 |--------+---------+---------+---------+---------+---------+---------+---------+---------+---------+---------+---------+---------|
ENSMUST00000113051 SYAARHRERPSWSSLDQKRFCRPQTNSSGSQKTPFAEDQLHTVPERSPENSPPVKSKHNYTQKAQPGQPLLPTGIYPVPSPEPHFAQVPQPSVSSNGTVYPALVKESGYTAAQGTCNKMATLDENGNQ
ENSMUST00000113054 SYAARHRERPSWSSLDQKRFCRPQTNSSGSQKTPFAEDQLHTVPERSPENSPPVKSKHNYTQKAQPGQPLLPTGIYPVPSPEPHFAQVPQPSVSSNGTVYPALVKESGYTAAQGTCNKMATLDENGNQ
ENSMUST00000113055 SYAARHRERPSWSSLDQKRFCRPQTNSSGSQKTPFAEDQLHTVPERSPENSPPVKSKHNYTQKAQPGQPLLPTGIYPVPSPEPHFAQVPQPSVSSNGTVYPALVKESGYTAAQGTCNKMATLDENGNQ
ENSMUST00000225438 SYAARHRERPSWSSLDQKRFCRPQTNSSGSQKTPFAEDQLHTVPERSPENSPPVKSKHNYTQKAQPGQPLLPTGIYPVPSPEPHFAQVPQPSVSSNGTVYPALVKESGYTAAQGTCNKMATLDENGNQ
        Consensus  SYAARHRERPSWSSLDQKRFCRPQTNSSGSQKTPFAEDQLHTVPERSPENSPPVKSKHNYTQKAQPGQPLLPTGIYPVPSPEPHFAQVPQPSVSSNGTVYPALVKESGYTAAQGTCNKMATLDENGNQ

                 521     530       540       550       560       570       580       590       600       610       620       630       640       650
                 |--------+---------+---------+---------+---------+---------+---------+---------+---------+---------+---------+---------+---------|
ENSMUST00000113051 NEASRPGFAFCQPLEHNSVTPVEKRPEPTAKYIYKVHFSSVPENEDSSLKRHITPPHGHSPYSERKNIHGGSRACSNHHSLSSPQAQALHYGDDRRPSRLSQPWEGDFQEDHNANLRQKYEREGQGQGL
ENSMUST00000113054 NEASRPGFAFCQPLEHNSVTPVEKRPEPTAKYIYKVHFSSVPENEDSSLKRHITPPHGHSPYSERKNIHGGSRACSNHHSLSSPQAQALHYGDDRRPSRLSQPWEGDFQEDHNANLRQKYEREGQGQGL
ENSMUST00000113055 NEASRPGFAFCQPLEHNSVTPVEKRPEPTAKYIYKVHFSSVPENEDSSLKRHITPPHGHSPYSERKNIHGGSRACSNHHSLSSPQAQALHYGDDRRPSRLSQPWEGDFQEDHNANLRQKYEREGQGQGL
ENSMUST00000225438 NEASRPGFAFCQPLEHNSVTPVEKRPEPTAKYIYKVHFSSVPENEDSSLKRHITPPHGHSPYSERKNIHGGSRACSNHHSLSSPQAQALHYGDDRRPSRLSQPWEGDFQEDHNANLRQKYEREGQGQGL
        Consensus  NEASRPGFAFCQPLEHNSVTPVEKRPEPTAKYIYKVHFSSVPENEDSSLKRHITPPHGHSPYSERKNIHGGSRACSNHHSLSSPQAQALHYGDDRRPSRLSQPWEGDFQEDHNANLRQKYEREGQGQGL

                 651     660       670       680       690       700       710       720       730       740       750       760       770       780
                 |--------+---------+---------+---------+---------+---------+---------+---------+---------+---------+---------+---------+---------|
ENSMUST00000113051 SGNSGRTRSAFSSLQNIPESLRRQSNVELGEAQEVHPGGRSKVEDPGRKAGASDIRGYLDRSVSYPRPEGKMNAYDSYHSADSRYEESPAPALPQTSGASQRRLSSSSSAAPQYRKPHCSYLEKVSRIEE
ENSMUST00000113054 SGNSGRTRSAFSSLQNIPESLRRQSNVELGEAQEVHPGGRSKVEDPGRKAGASDIRGYLDRSVSYPRPEGKMNAYDSYHSADSRYEESPAPALPQTSGASQRRLSSSSSAAPQYRKPHCSYLEKVSRIEE
ENSMUST00000113055 SGNSGRTRSAFSSLQNIPESLRRQSNVELGEAQEVHPGGRSKVEDPGRKAGASDIRGYLDRSVSYPRPEGKMNAYDSYHSADSRYEESPAPALPQTSGASQRRLSSSSSAAPQYRKPHCSYLEKVSRIEE
ENSMUST00000225438 SGNSGRTRSAFSSLQNIPESLRRQSNVELGEAQEVHPGGRSKVEDPGRKAGASDIRGYLDRSVSYPRPEGKMNAYDSYHSADSRYEESPAPALPQTSGASQRRLSSSSSAAPQYRKPHCSYLEKVSRIEE
        Consensus  SGNSGRTRSAFSSLQNIPESLRRQSNVELGEAQEVHPGGRSKVEDPGRKAGASDIRGYLDRSVSYPRPEGKMNAYDSYHSADSRYEESPAPALPQTSGASQRRLSSSSSAAPQYRKPHCSYLEKVSRIEE

                 781     790       800       810       820       830       840       850       860       870       880       890       900       910
                 |--------+---------+---------+---------+---------+---------+---------+---------+---------+---------+---------+---------+---------|
ENSMUST00000113051 REQGRHRPLSVGSSAYGPGYRPGRTGPTPSTSSSDLDDPKAGSVHFSESTEHLRNGEQNPPNGEAKQEEASRPQCSHLIRRAPADGRGPPARGGEPSRPEARLLRSQSTFQLYSEAEREASWSEDRPGTP
ENSMUST00000113054 REQGRHRPLSVGSSAYGPGYRPGRTGPTPSTSSSDLDDPKAGSVHFSESTEHLRNGEQNPPNGEAKQEEASRPQCSHLIRRAPADGRGPPARGGEPSRPEARLLRSQSTFQLYSEAEREASWSEDRPGTP
ENSMUST00000113055 REQGRHRPLSVGSSAYGPGYRPGRTGPTPSTSSSDLDDPKAGSVHFSESTEHLRNGEQNPPNGEAKQEEASRPQCSHLIRRAPADGRGPPARGGEPSRPEARLLRSQSTFQLYSEAEREASWSEDRPGTP
ENSMUST00000225438 REQGRHRPLSVGSSAYGPGYRPGRTGPTPSTSSSDLDDPKAGSVHFSESTEHLRNGEQNPPNGEAKQEEASRPQCSHLIRRAPADGRGPPARGGEPSRPEARLLRSQSTFQLYSEAEREASWSEDRPGTP
        Consensus  REQGRHRPLSVGSSAYGPGYRPGRTGPTPSTSSSDLDDPKAGSVHFSESTEHLRNGEQNPPNGEAKQEEASRPQCSHLIRRAPADGRGPPARGGEPSRPEARLLRSQSTFQLYSEAEREASWSEDRPGTP

                 911     920       930       940       950       960       970       980       990      1000      1010      1020      1030      1040
                 |--------+---------+---------+---------+---------+---------+---------+---------+---------+---------+---------+---------+---------|
ENSMUST00000113051 ESPLLDAPFSRAYRNSIKDAQSRVLGATSFRRRDLEPGTPATSRPWRPRPASAHVGMRSPEAAVPSSSPHTPRERHSVTPAAPQAARRGPRRRLTVEQKKRSYSEPEKMNEVGVSEEAEPTPCGPPRPAQ
ENSMUST00000113054 ESPLLDAPFSRAYRNSIKDAQSRVLGATSFRRRDLEPGTPATSRPWRPRPASAHVGMRSPEAAVPSSSPHTPRERHSVTPAAPQAARRGPRRRLTVEQKKRSYSEPEKMNEVGVSEEAEPTPCGPPRPAQ
ENSMUST00000113055 ESPLLDAPFSRAYRNSIKDAQSRVLGATSFRRRDLEPGTPATSRPWRPRPASAHVGMRSPEAAVPSSSPHTPRERHSVTPAAPQAARRGPRRRLTVEQKKRSYSEPEKMNEVGVSEEAEPTPCGPPRPAQ
ENSMUST00000225438 ESPLLDAPFSRAYRNSIKDAQSRVLGATSFRRRDLEPGTPATSRPWRPRPASAHVGMRSPEAAVPSSSPHTPRERHSVTPAAPQAARRGPRRRLTVEQKKRSYSEPEKMNEVGVSEEAEPTPCGPPRPAQ
        Consensus  ESPLLDAPFSRAYRNSIKDAQSRVLGATSFRRRDLEPGTPATSRPWRPRPASAHVGMRSPEAAVPSSSPHTPRERHSVTPAAPQAARRGPRRRLTVEQKKRSYSEPEKMNEVGVSEEAEPTPCGPPRPAQ

                1041    1050      1060      1070      1080      1090      1100      1110      1120      1130      1140      1150      1160      1170
                 |--------+---------+---------+---------+---------+---------+---------+---------+---------+---------+---------+---------+---------|
ENSMUST00000113051 PRFSESTVADRRRIFERDGKACSTLSLSGPELKQFQQSALADYIQRKTGKRPTGAACTPEAGLRERAQSAYLQAGPAAPDGPGLASACSLSSLREPEALPRKEHTHPSAADGPQAPRDRSSSFASGRLVG
ENSMUST00000113054 PRFSESTVADRRRIFERDGKACSTLSLSGPELKQFQQSALADYIQRKTGKRPTGAACTPEAGLRERAQSAYLQAGPAAPDGPGLASACSLSSLREPEALPRKEHTHPSAADGPQAPRDRSSSFASGRLVG
ENSMUST00000113055 PRFSESTVADRRRIFERDGKACSTLSLSGPELKQFQQSALADYIQRKTGKRPTGAACTPEAGLRERAQSAYLQAGPAAPDGPGLASACSLSSLREPEALPRKEHTHPSAADGPQAPRDRSSSFASGRLVG
ENSMUST00000225438 PRFSESTVADRRRIFERDGKACSTLSLSGPELKQFQQSALADYIQRKTGKRPTGAACTPEAGLRERAQSAYLQAGPAAPDGPGLASACSLSSLREPEALPRKEHTHPSAADGPQAPRDRSSSFASGRLVG
        Consensus  PRFSESTVADRRRIFERDGKACSTLSLSGPELKQFQQSALADYIQRKTGKRPTGAACTPEAGLRERAQSAYLQAGPAAPDGPGLASACSLSSLREPEALPRKEHTHPSAADGPQAPRDRSSSFASGRLVG

                1171    1180      1190      1200      1210      1220      1230      1240      1250      1260      1270      1280      1290      1300
                 |--------+---------+---------+---------+---------+---------+---------+---------+---------+---------+---------+---------+---------|
ENSMUST00000113051 ERRRWDPQVPRQLLSGANCEPRGVQRMDGAPGGPPSWGMVAGKAGKSKSAEDLLERSDTLAVPVHVRSRSSPTSDKKGQDVLLREGSNFGFVKDPCCLAGPGPRSLSCSDKGQNELALPLHHPTPCWNGS
ENSMUST00000113054 ERRRWDPQVPRQLLSGANCEPRGVQRMDGAPGGPPSWGMVAGKAGKSKSAEDLLERSDTLAVPVHVRSRSSPTSDKKGQDVLLREGSNFGFVKDPCCLAGPGPRSLSCSDKGQNELALPLHHPTPCWNGS
ENSMUST00000113055 ERRRWDPQVPRQLLSGANCEPRGVQRMDGAPGGPPSWGMVAGKAGKSKSAEDLLERSDTLAVPVHVRSRSSPTSDKKGQDVLLREGSNFGFVKDPCCLAGPGPRSLSCSDKGQNELALPLHHPTPCWNGS
ENSMUST00000225438 ERRRWDPQVPRQLLSGANCEPRGVQRMDGAPGGPPSWGMVAGKAGKSKSAEDLLERSDTLAVPVHVRSRSSPTSDKKGQDVLLREGSNFGFVKDPCCLAGPGPRSLSCSDKGQNELALPLHHPTPCWNGS
        Consensus  ERRRWDPQVPRQLLSGANCEPRGVQRMDGAPGGPPSWGMVAGKAGKSKSAEDLLERSDTLAVPVHVRSRSSPTSDKKGQDVLLREGSNFGFVKDPCCLAGPGPRSLSCSDKGQNELALPLHHPTPCWNGS

                1301    1310      1320      1330      1340      1350      1360      1370      1380      1390      1400      1410      1420      1430
                 |--------+---------+---------+---------+---------+---------+---------+---------+---------+---------+---------+---------+---------|
ENSMUST00000113051 GCKATVASSAPPESSGAADHLKQRRAPGPRPLSAGMHGHFPDARAASLSSPLPSPVPSSYRSQLAMDQQTGQQPPSSPASAYTQPTSPRSPELSSPAYGLGEGMWKRTSLPQRPPPPWVKWAHAYREDGL
ENSMUST00000113054 GCKATVASSAPPESSGAADHLKQRRAPGPRPLSAGMHGHFPDARAASLSSPLPSPVPSSYRSQLAMDQQTGQQPPSSPASAYTQPTSPRSPELSSPAYGLGEGMWKRTSLPQRPPPPWVKWAHAYREDGL
ENSMUST00000113055 GCKATVASSAPPESSGAADHLKQRRAPGPRPLSAGMHGHFPDARAASLSSPLPSPVPSSYRSQLAMDQQTGQQPPSSPASAYTQPTSPRSPELSSPAYGLGEGMWKRTSLPQRPPPPWVKWAHAYREDGL
ENSMUST00000225438 GCKATVASSAPPESSGAADHLKQRRAPGPRPLSAGMHGHFPDARAASLSSPLPSPVPSSYRSQLAMDQQTGQQPPSSPASAYTQPTSPRSPELSSPAYGLGEGMWKRTSLPQRPPPPWVKWAHAYREDGL
        Consensus  GCKATVASSAPPESSGAADHLKQRRAPGPRPLSAGMHGHFPDARAASLSSPLPSPVPSSYRSQLAMDQQTGQQPPSSPASAYTQPTSPRSPELSSPAYGLGEGMWKRTSLPQRPPPPWVKWAHAYREDGL

                1431    1440      1450      1460      1470      1480      1490      1500      1510      1520      1530      1540      1550      1560
                 |--------+---------+---------+---------+---------+---------+---------+---------+---------+---------+---------+---------+---------|
ENSMUST00000113051 AEDTLAPEFANLKHYRNQPSRPSSCSTSDPDTPGRISLRISESALQPSPPPRGDYDDEVFMKDLHPKVTSSPTFEALPPPPPPSPPSEEPLVNGTDDFPPPPPPQALCEVLLDGEASTEAGSGPCRIPRV
ENSMUST00000113054 AEDTLAPEFANLKHYRNQPSRPSSCSTSDPDTPGRISLRISESALQPSPPPRGDYDDEVFMKDLHPKVTSSPTFEALPPPPPPSPPSEEPLVNGTDDFPPPPPPQALCEVLLDGEASTEAGSGPCRIPRV
ENSMUST00000113055 AEDTLAPEFANLKHYRNQPSRPSSCSTSDPDTPGRISLRISESALQPSPPPRGDYDDEVFMKDLHPKVTSSPTFEALPPPPPPSPPSEEPLVNGTDDFPPPPPPQALCEVLLDGEASTEAGSGPCRIPRV
ENSMUST00000225438 AEDTLAPEFANLKHYRNQPSRPSSCSTSDPDTPGRISLRISESALQPSPPPRGDYDDEVFMKDLHPKVTSSPTFEALPPPPPPSPPSEEPLVNGTDDFPPPPPPQALCEVLLDGEASTEAGSGPCRIPRV
        Consensus  AEDTLAPEFANLKHYRNQPSRPSSCSTSDPDTPGRISLRISESALQPSPPPRGDYDDEVFMKDLHPKVTSSPTFEALPPPPPPSPPSEEPLVNGTDDFPPPPPPQALCEVLLDGEASTEAGSGPCRIPRV

                1561    1570      1580      1590      1600      1610      1620      1630      1640      1650      1660      1670      1680      1690
                 |--------+---------+---------+---------+---------+---------+---------+---------+---------+---------+---------+---------+---------|
ENSMUST00000113051 MYTREGHYPGAAHSEGSQIMTATPPQTSAKGSEAESNTPSSASAQPQLNGSPGKQLCPSQTRNLTYEPVERTQDLGKKTHAEPQKTSEDIRTEALAKEIVHQDKSLADILDPDSRMKTTMDLMEGLFPGD
ENSMUST00000113054 MYTREGHYPGAAHSEGSQIMTATPPQTSAKGSEAESNTPSSASAQPQLNGSPGKQLCPSQTRNLTYEPVERTQDLGKKTHAEPQKTSEDIRTEALAKEIVHQDKSLADILDPDSRMKTTMDLMEGLFPGD
ENSMUST00000113055 MYTREGHYPGAAHSEGSQIMTATPPQTSAKGSEAESNTPSSASAQPQLNGSPGKQLCPSQTRNLTYEPVERTQDLGKKTHAEPQKTSEDIRTEALAKEIVHQDKSLADILDPDSRMKTTMDLMEGLFPGD
ENSMUST00000225438 MYTREGHYPGAAHSEGSQIMTATPPQTSAKGSEAESNTPSSASAQPQLNGSPGKQLCPSQTRNLTYEPVERTQDLGKKTHAEPQKTSEDIRTEALAKEIVHQDKSLADILDPDSRMKTTMDLMEGLFPGD
        Consensus  MYTREGHYPGAAHSEGSQIMTATPPQTSAKGSEAESNTPSSASAQPQLNGSPGKQLCPSQTRNLTYEPVERTQDLGKKTHAEPQKTSEDIRTEALAKEIVHQDKSLADILDPDSRMKTTMDLMEGLFPGD

                1691    1700      1710      1720      1730      1740      1750      1760      1770      1780      1790      1800      1810      1820
                 |--------+---------+---------+---------+---------+---------+---------+---------+---------+---------+---------+---------+---------|
ENSMUST00000113051 ASVLMDSGAKRKALDITARRAGCEAKASDHKEAVSVLVNCPAYYSVSAAKAELLNKIKDMPEELQEEEGQEDVNEKKAELIGSLTHKLESLQEAKGSLLTDIKLNNALGEEVEALISELCKPNEFDKYKM
ENSMUST00000113054 ASVLMDSGAKRKALDITARRAGCEAKASDHKEAVSVLVNCPAYYSVSAAKAELLNKIKDMPEELQEEEGQEDVNEKKAELIGSLTHKLESLQEAKGSLLTDIKLNNALGEEVEALISELCKPNEFDKYKM
ENSMUST00000113055 ASVLMDSGAKRKALDITARRAGCEAKASDHKEAVSVLVNCPAYYSVSAAKAELLNKIKDMPEELQEEEGQEDVNEKKAELIGSLTHKLESLQEAKGSLLTDIKLNNALGEEVEALISELCKPNEFDKYKM
ENSMUST00000225438 ASVLMDSGAKRKALDITARRAGCEAKASDHKEAVSVLVNCPAYYSVSAAKAELLNKIKDMPEELQEEEGQEDVNEKKAELIGSLTHKLESLQEAKGSLLTDIKLNNALGEEVEALISELCKPNEFDKYKM
        Consensus  ASVLMDSGAKRKALDITARRAGCEAKASDHKEAVSVLVNCPAYYSVSAAKAELLNKIKDMPEELQEEEGQEDVNEKKAELIGSLTHKLESLQEAKGSLLTDIKLNNALGEEVEALISELCKPNEFDKYKM

                1821    1830      1840      1850      1860      1870      1880      1890      1900      1910      1920      1930      1940      1950
                 |--------+---------+---------+---------+---------+---------+---------+---------+---------+---------+---------+---------+---------|
ENSMUST00000113051 FIGDLDKVVNLLLSLSGRLARVENVLRGLGEDASKEERSSLNEKRKVLAGQHEDARELKENLDRRERVVLDILANYLSAEQLQDYQHFVKMKSTLLIEQRKLDDKIKLGQEQVRCLLESLPSDFRPKAGA
ENSMUST00000113054 FIGDLDKVVNLLLSLSGRLARVENVLRGLGEDASKEERSSLNEKRKVLAGQHEDARELKENLDRRERVVLDILANYLSAEQLQDYQHFVKMKSTLLIEQRKLDDKIKLGQEQVRCLLESLPSDFRPKAGA
ENSMUST00000113055 FIGDLDKVVNLLLSLSGRLARVENVLRGLGEDASKEERSSLNEKRKVLAGQHEDARELKENLDRRERVVLDILANYLSAEQLQDYQHFVKMKSTLLIEQRKLDDKIKLGQEQVRCLLESLPSDFRPKAGA
ENSMUST00000225438 FIGDLDKVVNLLLSLSGRLARVENVLRGLGEDASKEERSSLNEKRKVLAGQHEDARELKENLDRRERVVLDILANYLSAEQLQDYQHFVKMKSTLLIEQRKLDDKIKLGQEQVRCLLESLPSDFRPKAGA
        Consensus  FIGDLDKVVNLLLSLSGRLARVENVLRGLGEDASKEERSSLNEKRKVLAGQHEDARELKENLDRRERVVLDILANYLSAEQLQDYQHFVKMKSTLLIEQRKLDDKIKLGQEQVRCLLESLPSDFRPKAGA

                1951    1960      1970      1980
                 |--------+---------+---------|
ENSMUST00000113051 ISLPPALTGHGTPGGTSVFGGVFPTLTSPL
ENSMUST00000113054 ISLPPALTGHGTPGGTSVFGGVFPTLTSPL
ENSMUST00000113055 ISLPPALTGHGTPGGTSVFGGVFPTLTSPL
ENSMUST00000225438 ISLPPALTGHGTPGGTSVFGGVFPTLTSPL
        Consensus  ISLPPALTGHGTPGGTSVFGGVFPTLTSPL
```

Fig. S7: Mouse SHROOM3 protein sequence.

Protein sequence alignment of all murine SHROOM3 isoforms.

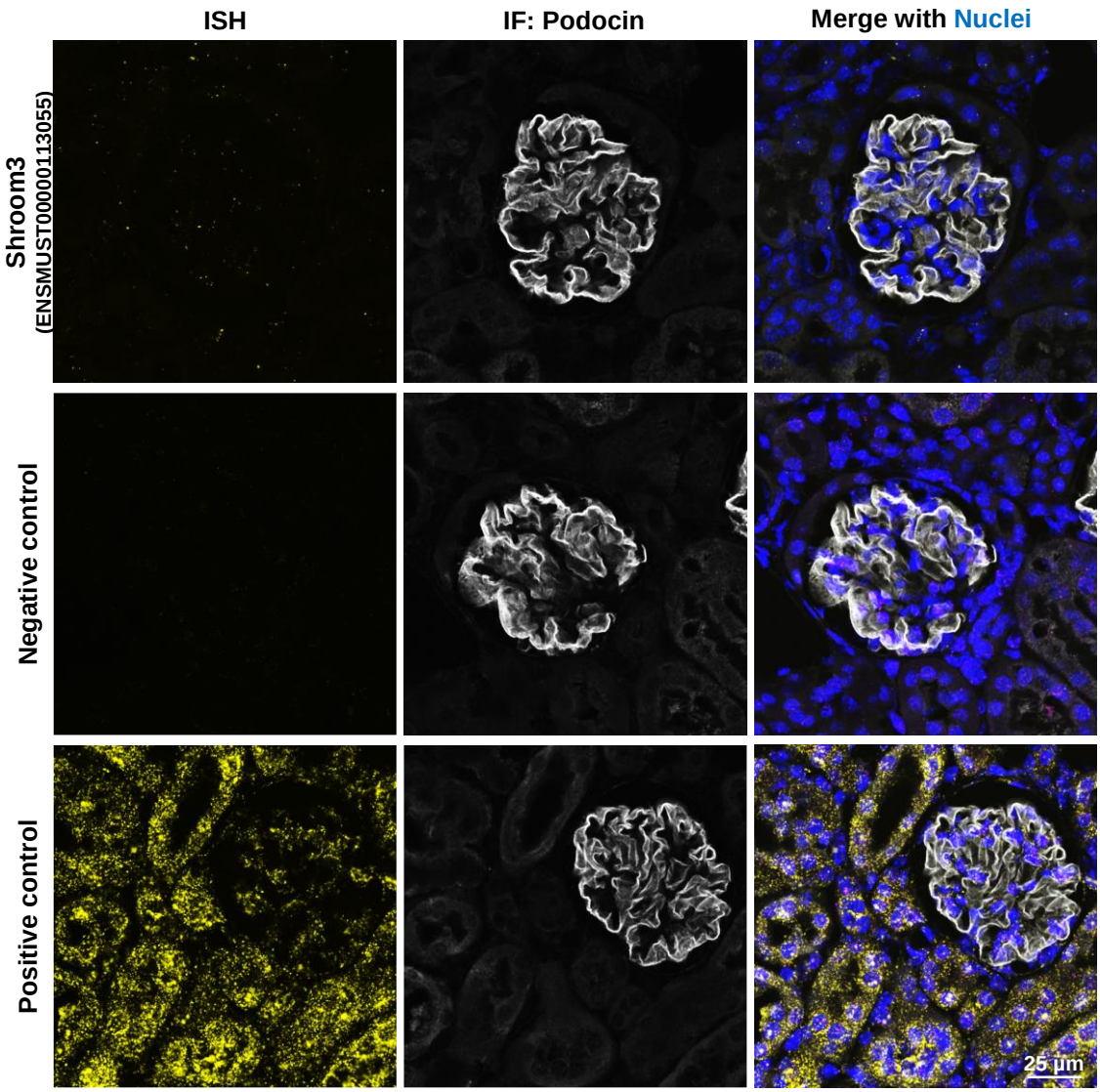

Fig. S8: RNAscope® ISH Assay.
In situ hybridization of the *Shroom3* coded isoform ENSMUST00000113055 in mouse kidney (yellow dots). Immunostaining of podocin is shown in white. Nuclei stained with HOECHST (blue). The negative control (*dapB*) and the positive control (*Ppib*) are also shown. Scale bar represents 25 µm.

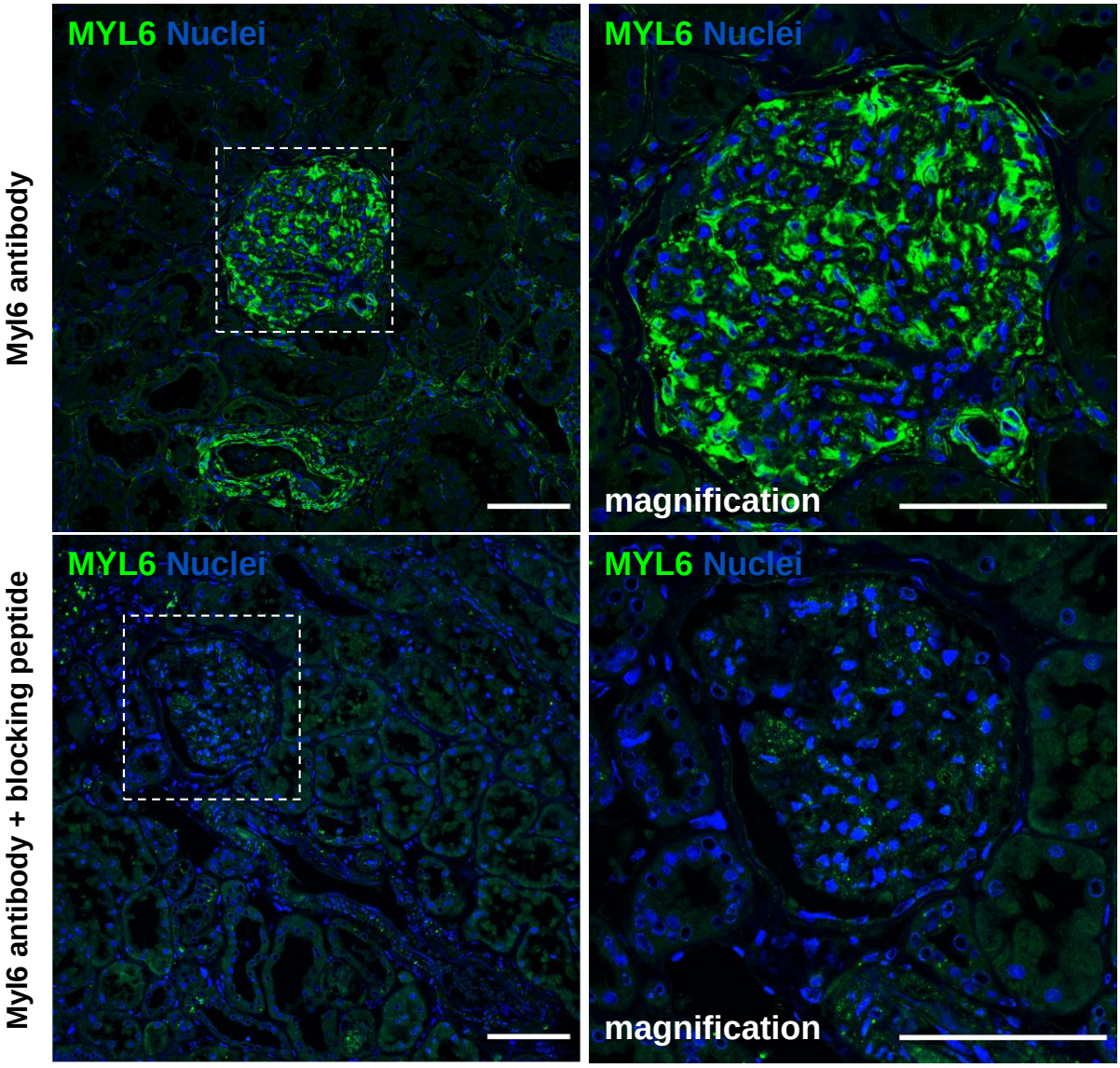

Fig. S9: MYL6 antibody verification.
Immunofluorescence staining with anti-MYL6 antibody (shown in green) in mouse kidney tissue. The specificity of the MYL6 antibody was successfully demonstrated by the use of a MYL6 blocking peptide (lower panel). Nuclei were stained with HOECHST (blue). Scale bars represent 50 µm.

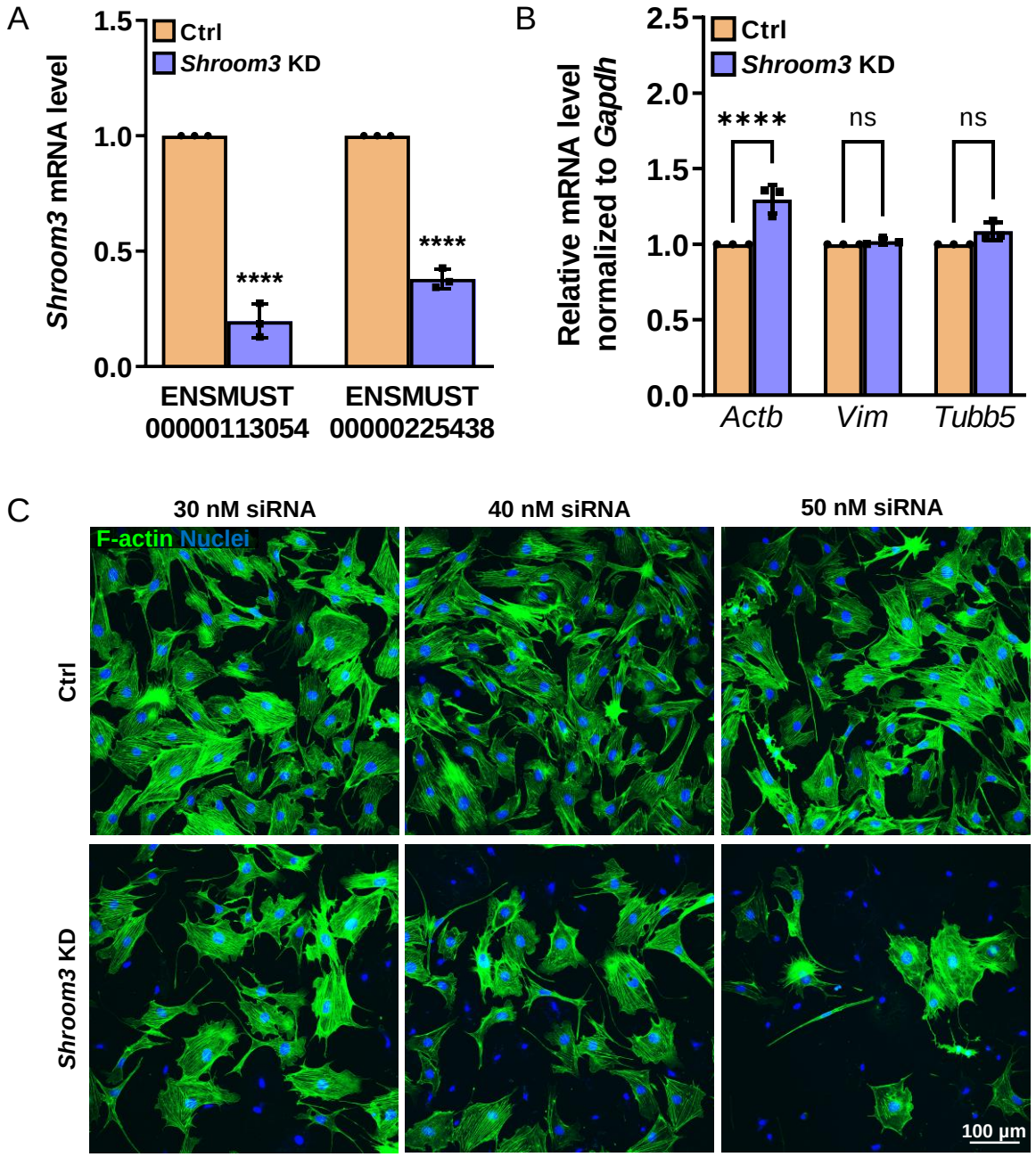

Fig. S10: *Shroom3* Knockdown (KD) in cultured murine podocytes
(A) qRT-PCR quantification of *Shroom3* knockdown (*Shroom3* KD) podocytes showed a significant decrease of *Shroom3* coded transcript expression levels compared to the control (Ctrl). (B) Beta-Actin (*Actb*) mRNA level was significantly up-regulated in Shroom3 KD podocytes. In contrast, the mRNA level of vimentin (*Vim*) as a marker of intermediate filaments and β-tubulin (*Tubb5*) were not changed significantly. Data are normalized against Ctrl KD and Gapdh and presented as means ± SD. (C) With an increased siRNA concentration the number of cells without visible F-actin increased dramatically in *Shroom3* KD podocytes. F-Actin is shown in green. Nuclei were stained with DAPI (blue). Scale bar represents 100 µm. ** $p<0.01$; **** $p<0.0001$.